Article

Neuron

# Toll Receptors Instruct Axon and Dendrite Targeting and Participate in Synaptic Partner Matching in a *Drosophila* Olfactory Circuit

## Highlights

- RNAi screen uncovers the Toll-family receptors Toll-6 and Toll-7 in neuronal wiring
- Toll-6 and Toll-7 instruct targeting of specific dendrites and axons, respectively
- Toll-6/7 mediate synaptic partner matching through heterophilic molecular partners
- Toll-6/7 function in neuronal wiring does not require canonical signaling pathway

## Authors

Alex Ward, Weizhe Hong, Vincenzo Favaloro, Liqun Luo

## Correspondence

alexward@stanford.edu (A.W.), lluo@stanford.edu (L.L.)

## In Brief

Ward et al. show that two members of the Toll receptor family instruct wiring specificity in the *Drosophila* olfactory circuit using novel signaling mechanisms. This study also reveals dynamic and long-range interactions between synaptic partners.

Ward et al., 2015, Neuron *85*, 1013–1028
March 4, 2015 
http://dx.doi.org/10.1016/j.neuron.2015.02.003

CellPress

Neuron
Article

# Toll Receptors Instruct Axon and Dendrite Targeting and Participate in Synaptic Partner Matching in a *Drosophila* Olfactory Circuit

Alex Ward,[1,3,*] Weizhe Hong,[1,2,3] Vincenzo Favaloro,[1] and Liqun Luo[1,*]
[1]Howard Hughes Medical Institute and Department of Biology, Stanford University, Stanford, CA 94305, USA
[2]Present address: Division of Biology and Biological Engineering, California Institute of Technology, Pasadena, CA 91125, USA
[3]Co-first author
*Correspondence: alexward@stanford.edu (A.W.), lluo@stanford.edu (L.L.)
http://dx.doi.org/10.1016/j.neuron.2015.02.003

## SUMMARY

**Our understanding of the mechanisms that establish wiring specificity of complex neural circuits is far from complete. During *Drosophila* olfactory circuit assembly, axons of 50 olfactory receptor neuron (ORN) classes and dendrites of 50 projection neuron (PN) classes precisely target to 50 discrete glomeruli, forming parallel information-processing pathways. Here we show that Toll-6 and Toll-7, members of the Toll receptor family best known for functions in innate immunity and embryonic patterning, cell autonomously instruct the targeting of specific classes of PN dendrites and ORN axons, respectively. The canonical ligands and downstream partners of Toll receptors in embryonic patterning and innate immunity are not required for the function of Toll-6/Toll-7 in wiring specificity, nor are their cytoplasmic domains. Interestingly, both Toll-6 and Toll-7 participate in synaptic partner matching between ORN axons and PN dendrites. Our investigations reveal that olfactory circuit assembly involves dynamic and long-range interactions between PN dendrites and ORN axons.**

## INTRODUCTION

Neuronal circuit assembly involves a coordinated sequence of developmental steps that culminates in the formation of precise connections between highly specific, often anatomically distant, groups of neurons. This necessitates mechanisms that (1) guide axons of presynaptic neurons near their targets, (2) direct the elaboration of dendrites of postsynaptic neurons within a target zone, (3) act locally to determine specificity of connections between axons and dendrites, and (4) recruit protein complexes required for synapse formation. While great progress has been made in our understanding of the mechanisms governing long-range axon guidance and synapse formation (Chia et al., 2013; Kolodkin and Tessier-Lavigne, 2011), the intermediate steps in which cognate pre- and post-synaptic partners identify one another locally among a multitude of incorrect choices remain less understood (Zipursky and Sanes, 2010).

From insects to mammals, the sensory and second order neurons in the olfactory system form parallel, discrete information processing channels, making them useful models for investigating the general mechanisms by which wiring specificity is established during development (Luo and Flanagan, 2007). In *Drosophila*, most of the 50 classes of olfactory receptor neurons (ORNs) each express a single olfactory receptor (OR) gene and target axons to a single invariant position in the antennal lobe termed a glomerulus (Couto et al., 2005; Fishilevich and Vosshall, 2005; Silbering et al., 2011). Projection neurons (PNs), which form the output of the antennal lobe, each arborize dendrites within a single glomerulus and receive direct inputs from axons of the corresponding ORN class (Jefferis et al., 2001; Stocker et al., 1990). Thus, the olfactory circuit exhibits highly specific one-to-one pairings between 50 ORN classes and 50 PN classes, presumably via cell surface recognition molecules. Previous work suggests that PN dendrites pre-pattern the developing antennal lobe. By 18 hr after pupae formation (APF), when pioneering ORN axons just contact the periphery of the developing antennal lobe, PNs have already elaborated dendrites within the antennal lobe and occupy areas corresponding to their future glomerular positions (Jefferis et al., 2004). The transmembrane semaphorin Sema-1a instructs coarse PN dendrite targeting along the dorsolateral-ventromedial axis in response to a gradient of secreted Sema-2a/Sema-2b (Komiyama et al., 2007; Sweeney et al., 2011). Locally acting determinants such as Capricious segregate PN dendrites into discrete glomeruli through a binary choice (Hong et al., 2009). Several distinct mechanisms of ORN axon targeting have also been identified. In addition to its role in PNs, Sema-1a mediates repulsive axon-axon interactions to segregate ORN axons originating from different sensory organs (Lattemann et al., 2007; Sweeney et al., 2007). Sema-2b and its receptor PlexB link Notch-dependent ORN cell fate decisions with axon trajectory choice and target selection (Joo et al., 2013). Hedgehog signaling coordinates peripheral ORN cell body position with antennal lobe glomerular targeting (Chou et al., 2010). Finally, recent work identified a matching mechanism that pairs pre-synaptic ORN axons with their cognate PN dendrite partners via Teneurin-mediated homophilic attraction (Hong et al., 2012).

Given the inherent complexity of wiring 50 ORN and PN classes, we anticipate that additional molecules and mechanisms regulate olfactory circuit assembly (Hong and Luo, 2014). Here we carried out a high-resolution RNAi screen to identify cell surface molecules required for olfactory circuit wiring specificity. We found that Toll-6 and Toll-7, two members of the Toll-family receptors best known for their conserved role as innate immunity receptors (Imler and Zheng, 2004; Takeda et al., 2003), instruct PN dendrite and ORN axon targeting, respectively. Toll-6 and Toll-7 also participate in partner matching of cognate pairs of PN dendrites and ORN axons, similar to our previous findings with the Teneurins (Hong et al., 2012), suggesting that multiple partner matching mechanisms are required for ensuring a robust wiring process. Analyses of the functions of these Toll receptors implied non-canonical signaling mechanisms and revealed that olfactory circuit assembly involves dynamic, long-range interactions between PN dendrites and ORN axons.

## RESULTS

### An RNAi Screen for Wiring Specificity Molecules in the Olfactory System Identifies the Toll-Family Receptors Toll-6 and Toll-7

To further elucidate the mechanisms that instruct PN dendrite and ORN axon targeting specificity in the *Drosophila* antennal lobe, we designed a high-resolution confocal-based RNAi screen of candidate transmembrane and secreted molecules (Figure 1A). To visualize PN dendrites, we utilized the Q-system driver *Mz19-QF*, which specifically labels two classes of PNs (DA1 and VA1d) that arborize dendrites at the anterior surface of the antennal lobe (Hong et al., 2012). Simultaneously, ORNs that express the Or88a odorant receptor and whose axons target to the VA1d glomerulus (hereafter VA1d ORNs) were labeled by the expression of myristolated tdTomato from the *Or88a-myr-tdT* transgene. Likewise, ORNs that express Or47b, and whose axons target to the adjacent VA1v glomerulus (also known as VA1lm), were labeled by the expression of rat CD2 from *Or47b-rCD2* (Figures 1A and 1B). In addition to these markers, we visualized the entire antennal lobe neuropil with an antibody against N-cadherin. Four-color confocal imaging enabled us to observe both matching and neighboring classes of PNs and ORNs and to identify defects in PN dendrite targeting, ORN axon targeting, axon segregation between neighboring ORN classes, and ORN axon–PN dendrite matching. The *C155-GAL4* driver line was used for pan-neuronal RNAi knockdown of predicted transmembrane and secreted proteins (Kurusu et al., 2008) (Figure 1A).

We screened a total of 768 lines representing 278 genes containing the following domain types: immunoglobulin (Ig), leucine-rich repeat (LRR), cadherin, fibronectin (FN), and epidermal growth factor (EGF) repeats. We identified two related LRR proteins, Toll-6 and Toll-7, which showed specific targeting defects of VA1d ORN axons and PN dendrites following RNAi knockdown of their respective genes. The VA1d glomerulus is located at the anterior surface of the lateral antennal lobe, ventral to the DA1 glomerulus and dorsal to the VA1v glomerulus (Figure 1B). *toll-6* RNAi knockdown caused a pronounced dorsal shift of VA1d PN dendrites and ORN axons, either medial (Figure 1C) or lateral (data not shown) to the DA1 glomerulus. On the other hand, *toll-7* RNAi knockdown consistently caused medial mistargeting of VA1d PN dendrites and ORN axons (Figure 1D).

Toll-family receptors are single-pass transmembrane proteins with extensive LRRs in their extracellular domain and a conserved Toll/interleukin-1 receptor (TIR) domain in the cytoplasmic region (Figure 1J). *Drosophila toll-6* and *toll-7* are expressed in the peripheral and central nervous system during development and are implicated in motor axon targeting and neuronal survival in embryos (McIlroy et al., 2013). To validate the RNAi phenotypes, we tested VA1d ORN axon targeting in *toll-6*- and *toll-7*-null mutants (see Experimental Procedures), both of which are viable. *toll-6* mutants exhibited dorsal mistargeting of VA1d ORN axons (Figure 1F, compared to Figure 1E; quantified in Figure 1H) similar to that caused by RNAi-mediated knockdown (Figure 1C). Likewise, *toll-7* mutants recapitulated the medial mistargeting of VA1d ORN axons (Figure 1G) observed in RNAi experiments (Figure 1D). We quantified VA1d ORN axon mistargeting by analyzing the distribution of fluorescence intensity across the antennal lobe (Komiyama et al., 2007). VA1d ORN axons displayed a significant medial shift in *toll-7* mutants compared with wild-type animals (Figure 1I).

In summary, the RNAi-based screen followed by loss-of-function mutant analysis identified two Toll-family receptors, Toll-6 and Toll-7, to be required for targeting of olfactory neuron processes to the VA1d glomerulus. We next explore the developmental mechanisms by which these Toll receptors regulate wiring specificity.

### Toll-7 Is Expressed in ORN Axons Targeting Anterolateral Glomeruli

To determine the spatial distribution of Toll-7 during development, we generated an antibody against Toll-7 and used it to stain developing antennal lobe. At 48 hr APF, dendrites of individual PNs and axons of individual ORNs have just coalesced into specific glomeruli and begin to be identifiable from neuropil staining (Jefferis et al., 2004). During this period of development, Toll-7 protein was enriched in a cluster of glomeruli in the anterior and lateral regions of the antennal lobe, which includes the DA1, VA1d, and VA1v glomeruli (Figures 2A–2C). Toll-7 signal was absent in *toll-7* mutants (Figure 2D), confirming antibody specificity.

To identify which cells produce Toll-7, we used a cell-type-specific RNAi knockdown approach. *Pebbled-GAL4* is broadly expressed in all ORNs but not in central neurons (Sweeney et al., 2007). Toll-7 staining was abrogated following *Pebbled-GAL4*-based RNAi knockdown of *toll-7* (Figure 2E), suggesting that Toll-7 is predominantly produced by ORNs. Indeed, we detected Toll-7 in the antennal commissure of wild-type pupae consisting mostly of commissural ORN axons (data not shown). Thus, Toll-7 is differentially expressed in ORN axons that innervate a cluster of anterolateral glomeruli, including VA1d ORN axons that display targeting defects in *toll-7* mutants.

### Toll-7 Acts Cell Autonomously in VA1d and DA1 ORNs to Control Axon Targeting

To identify which neurons require *toll-7* for VA1d ORN axon targeting, we first used cell-type-specific RNAi knockdown.

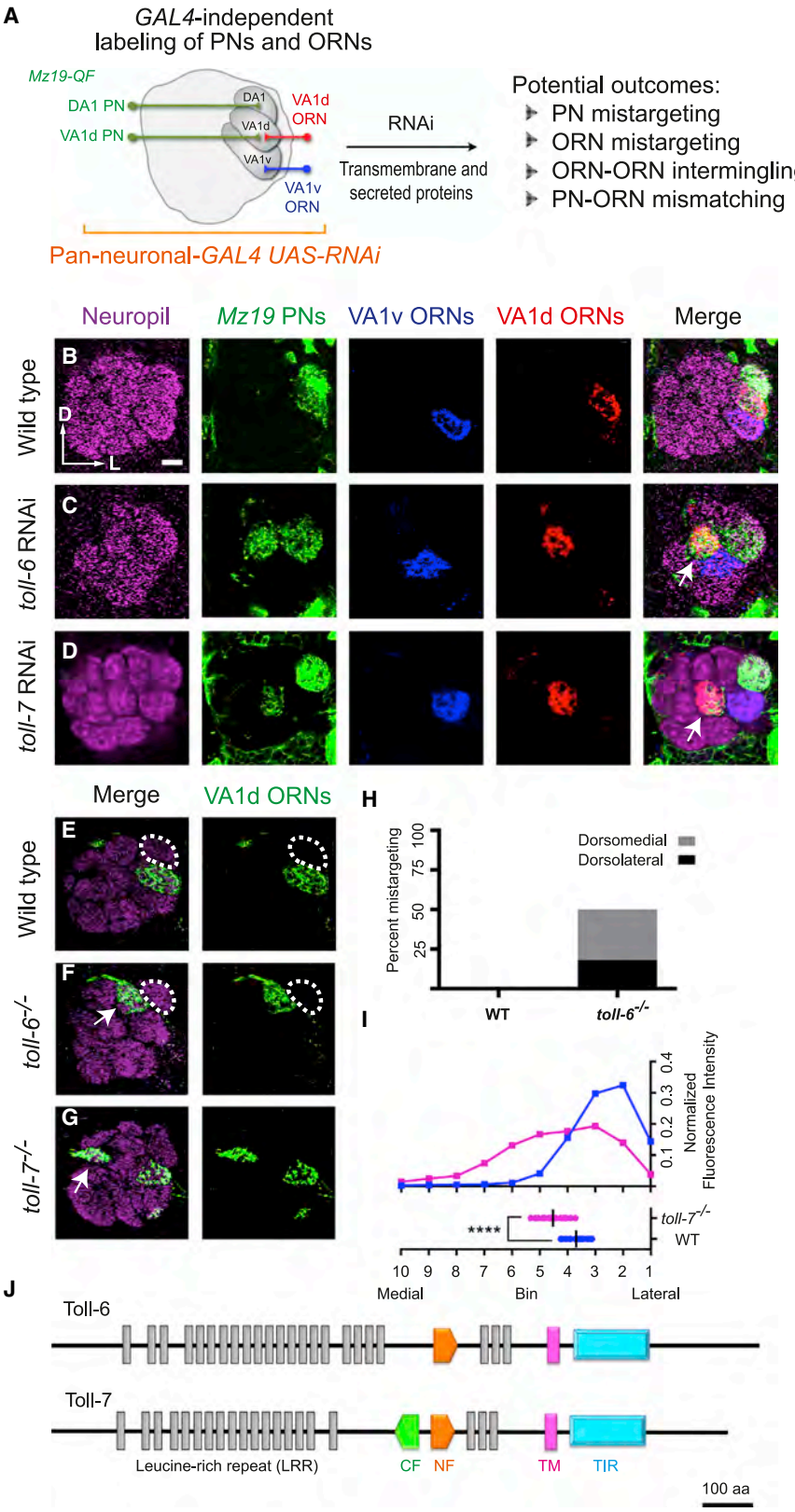


**Figure 1. Identification of Toll-6 and Toll-7 as Wiring Specificity Molecules in an RNAi Screen**

All images are single confocal sections of adult antennal lobes, with magenta showing neuropil staining and other colors showing axons of specific ORN classes and dendrites of specific PN classes as indicated. N is number of antennal lobes tested.

(A) Schematic of RNAi screen. A pan-neuronal *C155-GAL4* drives *UAS-RNAi* of predicted transmembrane and secreted molecules. Dendrites of two PN classes, DA1 and VA1d, are labeled by *Mz19QF* > *QUAS-mCD8GFP*. Axons of two ORN classes, VA1d and VA1v, are labeled by two different markers driven directly from odorant receptor promoters. This four-color screen can in principle identify phenotypes in four processes listed on the right.

(B) In wild-type, dendrites of *Mz19-QF*$^{+}$ PNs and axons of VA1d and VA1v ORNs target to their glomeruli in stereotyped positions in the lateral antennal lobe. D, dorsal; L, lateral (scale bar is 10 μm).

(C) Pan-neuronal RNAi knockdown of *toll-6* causes dorsomedial (shown here) or dorsolateral (not shown) mistargeting of VA1d ORN axons and PN dendrites (arrow).

(D) Pan-neuronal RNAi knockdown of *toll-7* causes VA1d ORN axons and PN dendrites to mistarget to a medial position.

(E) Wild-type VA1d ORNs target axons to the VA1d glomerulus ventral to the DA1 glomerulus (dashed circle).

(F) In *toll-6* mutants, VA1d ORN axons mistarget either dorsomedially (shown here) or dorsolaterally (see Figure 4I) in 50% of cases (n = 20).

(G) In *toll-7* mutants, VA1d ORN axons partially mistarget to a medial position. Mistargeting was observed in all antennal lobes examined (n = 24).

(H) Quantification of VA1d ORN axon mistargeting in *toll-6* mutants, shown as percent dorsomedial (gray) and dorsolateral (black) mistargeting.

(I) Quantification of VA1d ORN axon mistargeting in *toll-7* mutants. Top, normalized fluorescence intensity was binned along the lateral (bin 1) to medial (bin 10) axis of the antennal lobe and averaged across all animals (top graph). Bottom, mean intensity of VA1d ORN axons (each dot represents one fly; t test, $p < 0.0001$) is shifted medially in *toll-7* mutants (bottom graph).

(J) Schematic of the domain organization of Toll-6 and Toll-7 proteins. Toll-6 and Toll-7 both have extracellular LRR domains and intracellular conserved TIR domains. CF and NF, C-terminal and N-terminal LRR cysteine cluster motif. TM, transmembrane domain.

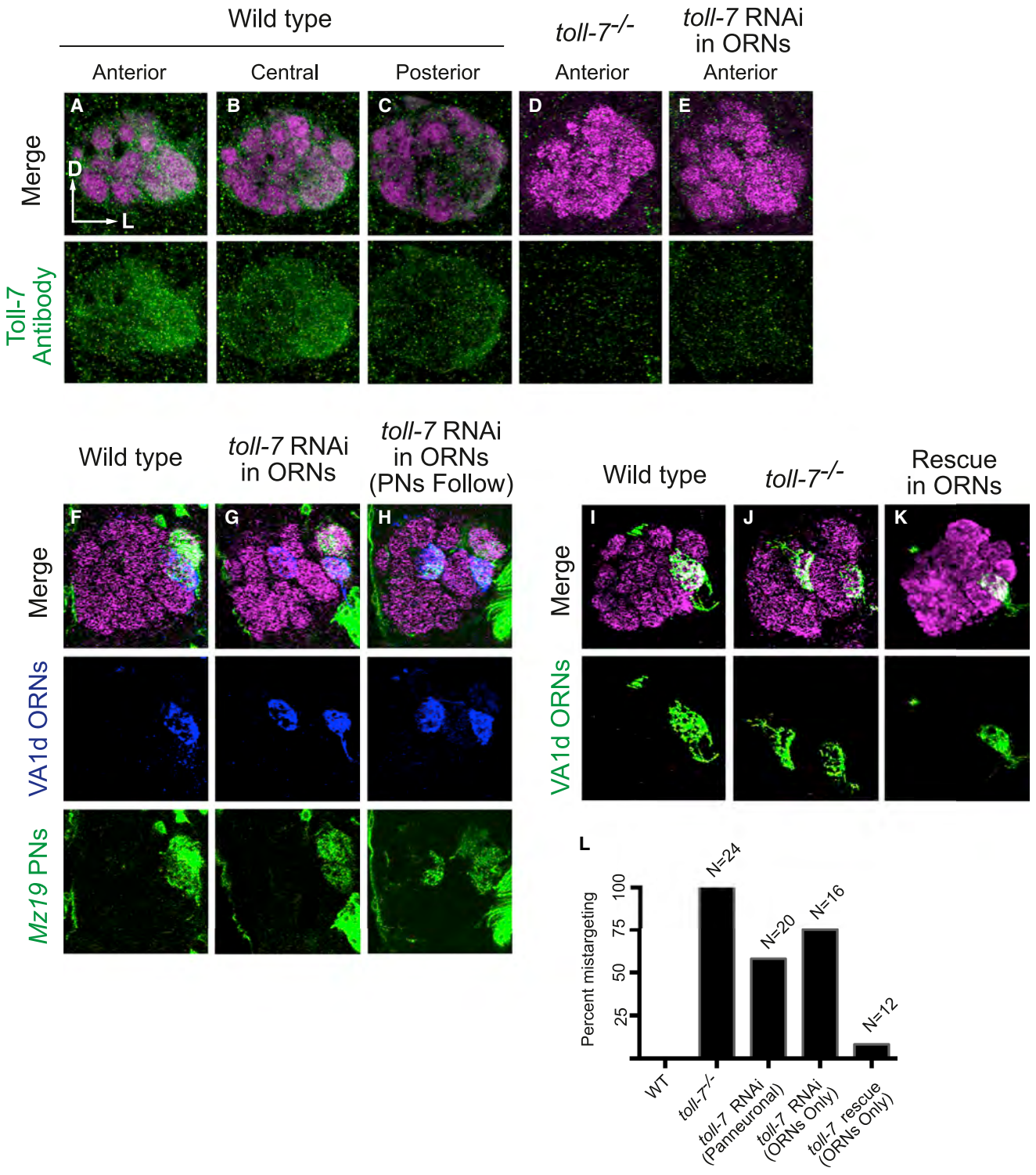


**Figure 2. Toll-7 Is Expressed in ORN Axons Targeting Anterolateral Glomeruli and Is Required in ORNs**

(A)–(E) Toll-7 antibody staining (green) and a merged image with neuropil staining (magenta) in the same single confocal section of antennal lobes at 48 hr APF. (F)–(K) Labeling of specific ORN and PN classes and a merged image with neuropil labeling of the same single confocal section of adult antennal lobes. (A–C) In anterior (A), middle (B), and posterior (C) sections of the antennal lobe, Toll-7 protein localizes to lateral glomeruli in the anterior and middle sections, including DA1, VA1d, and VA1v glomeruli, but is largely absent in the posterior section. Because of the limited strength of Toll-7 antibody staining, we were not able to determine the identity of all glomeruli that are Toll-7$^{+}$ unambiguously.

*(legend continued on next page)*

Knockdown of *toll-7* with the PN-specific driver *Mz19-GAL4* (expressed in VA1d, DC3, and DA1 PNs) had no effect on targeting of PN dendrites and ORN axons to VA1d (Figure S1A). Likewise, *toll-7*$^{-/-}$ VA1d PNs in *Mz19-GAL4*-based MARCM clones targeted their dendrites normally (Figure S1B). However, *toll-7* knockdown in ORNs using *Pebbled-GAL4* recapitulated the VA1d targeting defects observed with pan-neuronal RNAi (Figures 2F–2H and 2L). Expression of *UAS-toll-7* in ORNs using *Pebbled-GAL4* rescued VA1d ORN axon targeting defects observed in *toll-7* mutants (Figures 2I–2K and 2L), indicating that Toll-7 in ORNs is necessary and sufficient for proper VA1d wiring. ORN knockdown of *toll-7* also resulted in occasional PN dendrite mistargeting events (Figure 2H), indicating that mistargeted ORN axons can affect targeting of partner PN dendrites during development. This is surprising in light of our previous work showing that PN dendrites pre-pattern the antennal lobe to instruct target selection of later-arriving ORN axons (Jefferis et al., 2004). Our *toll-7* ORN-specific RNAi findings suggest that target selection of PN dendrites is more flexible than was previously appreciated and that the interactions of PN dendrites and ORN axons can mutually affect each other's final target selection.

In support of this, we simultaneously examined PN dendrites and ORN axons during antennal lobe development. We labeled DA1/VA1d PN dendrites using *Mz19-QF* and DM6/DL4 ORN axons using the enhancer trap *Am29-GAL4*, which is expressed early in pupae development (Endo et al., 2007; Joo et al., 2013). At 24–36 hr APF, both AM29$^{+}$ ORNs and *Mz19*$^{+}$ PNs extended fine branches to relatively broad areas in the antennal lobe, and these processes partially overlapped at 36 hr APF even though these ORNs and PNs are not synaptic partners (Figures S2A–S2C). This suggests that targeting of these PN dendrites and ORN axons is dynamic before their eventual coalescence into specific glomeruli between 42 and 48 hr APF (Figures S2D and S2E).

Having established that *toll-7* is required in ORNs alone for targeting to the VA1d glomerulus, we next tested whether *toll-7* functions cell autonomously in ORNs. We first employed MARCM to label VA1d ORN clones mutant for *toll-7* using *eyFLP*, which produces mutant clones in ORNs but not in their central targets (Hummel et al., 2003). *eyFLP*-based MARCM generated mosaic *toll-7*$^{-/-}$ clones in 30%–50% of ORNs from all classes, but only *toll-7*$^{-/-}$ VA1d ORN axons were visualized. *toll-7*$^{-/-}$ VA1d ORN axons mistargeted medially (Figures 3B and 3I), similar to phenotypes in *toll-7* RNAi and whole-animal mutants. Using *hsFLP*-based MARCM, we generated sparser mosaic *toll-7*$^{-/-}$ clones and again observed qualitatively similar mistargeting (Figures 3C and 3I). We also performed *eyFLP*-based reverse MARCM (Zhu and Luo, 2004), in which wild-type VA1d ORN axons are visualized in the background of large (30%–50% of all ORNs) mutant ORN clones. Despite the presence of these mutant ORNs, targeting of the labeled wild-type VA1d ORN axons was normal (Figures 3D and 3I). Together, these experiments indicate that Toll-7 functions cell autonomously for VA1d ORN axon targeting.

To determine whether *toll-7* is broadly required for ORN axon targeting or instead plays a specific role in only a subset of ORN classes, we performed whole-animal *toll-7* mutant analysis in different ORN classes using *Or-GAL4* driver lines. Interestingly, eight different ORN classes displayed significant targeting defects (Figure S3). Of these, DA1 is clearly Toll-7$^{+}$, and VA3 and VA7l may also be Toll-7$^{+}$ based on proximity to the Toll-7-enriched signal (Figures 2A–2C). To investigate whether *toll-7* acts cell autonomously in these ORN classes, we conducted *eyFLP* MARCM experiments using the same *Or-GAL4* driver lines. To our surprise, among the eight ORN classes examined, only DA1 ORNs displayed defects in axon targeting, whereas ORN axon targeting for the other classes was normal (data not shown). DA1 ORN axons mistargeted to a medial position of the antennal lobe (Figures 3F and 3J), similar to the phenotype exhibited by VA1d ORN axons. Medial DA1 ORN axon targeting defects were also observed with *toll-7*$^{-/-}$ *hsFLP* MARCM (Figures 3G and 3J), and targeting was normal when we visualized wild-type DA1 axons in *eyFLP*-based reverse MARCM experiments (Figures 3H and 3J). Therefore, *toll-7* acts cell autonomously in VA1d and DA1 ORNs, while the axon-targeting defects in ORN classes VA7l, DM3, DA2, VM7, VA3, VC1, and VM5v were likely due to cell-non-autonomous effects. These cell-non-autonomous effects could result from ORN axon-axon interactions (Sweeney et al., 2007) or from disrupted matching of ORN axons–PN dendrites (see below), which could cause unmatched PN dendrites to influence targeting/matching of other ORN axons.

## Expression of Toll-6 in Small Subsets of PNs Is Sufficient to Rescue VA1d ORN Axon Mistargeting

To determine the expression pattern of the other Toll receptor identified in our screen, Toll-6, we generated an antibody and stained the developing antennal lobe. Interestingly, Toll-6 was enriched in the lateral antennal lobe in many of the same glomeruli as seen with the Toll-7 antibody, including DA1, VA1d, and VA1v (Figures 4A–4C). Toll-6 is also found in DL3, DC3, DC1, DA4l, and DA4m glomeruli, which are all innervated by trichoid ORNs (Couto et al., 2005). These staining patterns were absent in *toll-6* mutant animals (Figure 4D), confirming antibody specificity.

We also examined the Toll-6 expression pattern using a putative *toll-6* enhancer trap line, *D42*, which has a GAL4-containing P

(D) Toll-7 antibody is specific as signal is absent in *toll-7* mutants.
(E) Toll-7 antibody signal is abrogated following RNAi knockdown of *toll-7* in ORNs using *Pebbled-GAL4*.
(F) In wild-type animals, VA1d ORN axons and *Mz19-QF*-labeled PN dendrites target the lateral antennal lobe.
(G) ORN-specific RNAi knockdown of *toll-7* by *Pebbled-GAL4* causes VA1d ORN axons to mistarget medially.
(H) Occasionally, *Mz19-QF*$^{+}$ (likely VA1d) PN dendrites mistarget medially following ORN-specific RNAi knockdown of *toll-7*. (n = 3/9 mistarget, VA1d PN dendrites were labeled in only 9 of the 16 antennal lobes in Figure 2G due to inconsistent *Mz19-QF* labeling.)
(I–K) VA1d ORN axon targeting in wild-type (K), *toll-7* mutant (L), and in *toll-7* mutant in which a *Toll-7* transgene is expressed in all ORNs with *Pebbled-GAL4* (K).
(L) Quantification of VA1d ORN axon mistargeting comparing *toll-7* mutants with tissue-specific RNAi and rescue.

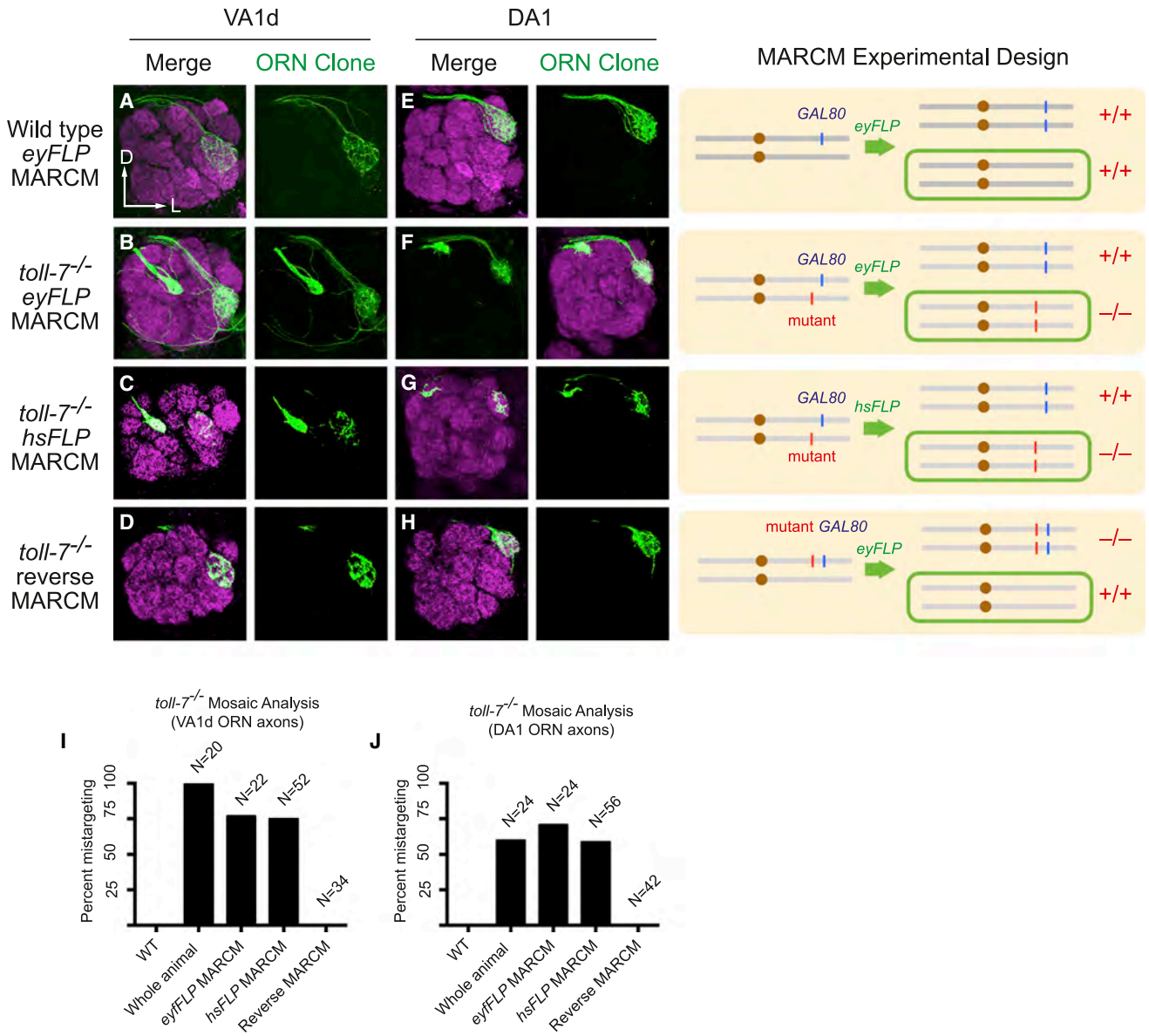


**Figure 3. Toll-7 Acts Cell Autonomously in VA1d and DA1 ORNs to Control Their Axon Targeting**

All images are confocal projections of adult antennal lobe showing MARCM labeling of VA1d ([A]–[D]) or DA1 ([E]–[H]) ORN axons in green and neuropil staining in magenta. The right panel shows the MARCM experimental design for each pair of images on the left; green rectangles indicate labeled cells.

(A and E) Wild-type VA1d (A) or DA1 (E) *eyFLP* MARCM labeled ORN clones target axons to the VA1d or DA1 glomerulus in the anterolateral antennal lobe.

(B and F) *toll-7*$^{-/-}$ VA1d (B) or DA1 (F) ORN axons in *eyFLP* MARCM clones partially mistarget to the medial antennal lobe. About 30%–50% of all ORN axons are *toll-7*$^{-/-}$ but only VA1d or DA1 ORNs are labeled.

(C and G) Smaller *toll-7*$^{-/-}$ VA1d (C) or DA1 (G) clones produced by *hsFLP* MARCM also display partial axon mistargeting to the medial antennal lobe.

(D and H) In *eyFLP* reverse MARCM clones, *toll-7*$^{-/-}$ VA1d (D) or DA1 (H) ORN axons target normally to the VA1d or DA1 glomerulus despite the presence of 30%–50% unlabeled *toll-7*$^{-/-}$ ORN axons.

(I and J) Quantification of VA1d (I) and DA1 (J) ORN axon mistargeting in *toll-6* whole-animal mutants, *eyFLP* MARCM clones, *hsFLP* MARCM clones, and reverse MARCM clones.

element inserted approximately 1.5 kb upstream of the *toll-6* transcriptional start site. *D42-GAL4* strongly labeled the same eight trichoid glomeruli observed with the Toll-6 antibody and weakly labeled a few additional glomeruli. Further, *D42-GAL4* labeled PN cell bodies as well as the antennal commissure and fasciculating ORN axons entering the antennal lobe (data not shown), suggesting that Toll-6 is expressed in both PNs and ORNs. To more precisely determine the cellular source of Toll-6, we employed an intersectional strategy using a FLP- and GAL4-dependent reporter. Intersections between *GH146-FLP*

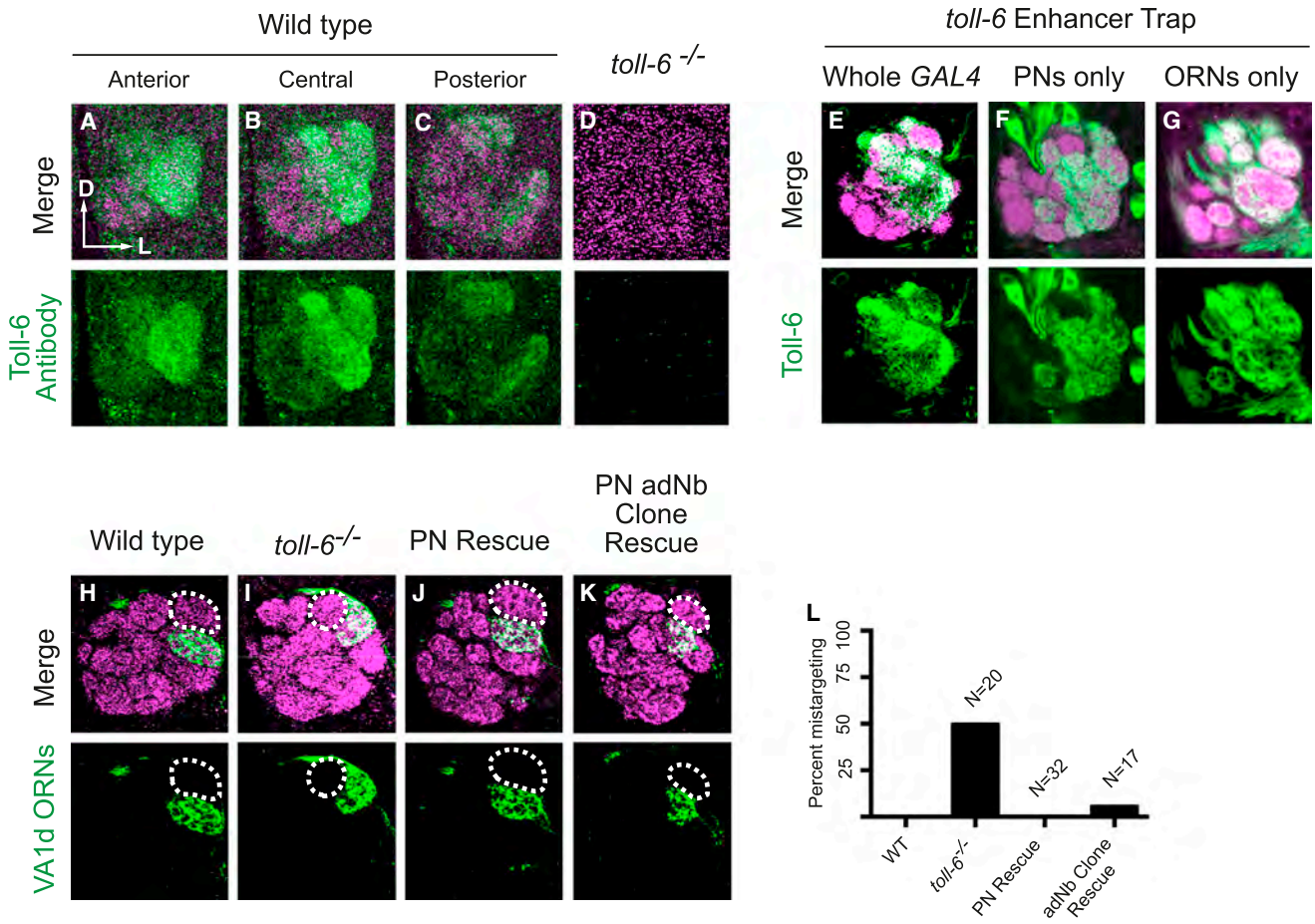


**Figure 4. Expression of Toll-6 in Small Subsets of PNs Is Sufficient to Rescue VA1d ORN Mistargeting**

(A–C) Single confocal section of anterior (A), middle (B), and posterior (C) antennal lobe at 48 hr APF stained with anti-Toll-6 antibody, revealing that Toll-6 is enriched in lateral glomeruli in the anterior and middle sections, including DA1, VA1d, and VA1v.

(D) Toll-6 antibody is specific as signal is absent in *toll-6* mutants.

(E) *D42-GAL4* staining recapitulates endogenous Toll-6 antibody staining in 48 hr APF antennal lobes.

(F and G) Intersection of *GH146-FLP* (F) or *eyFLP* (G) and *D42-GAL4* labels PN dendrites or ORN axons, respectively, targeting the glomeruli observed with endogenous *D42-GAL4*.

(H) Wild-type VA1d ORNs labeled by *Or88a-myr-tdTomato* (pseudocolored in green) target axons ventral to the DA1 glomerulus (dashed circle).

(I) In *toll-6* mutants, VA1d ORN axons mistarget dorsally, lateral to the DA1 glomerulus in this example (see also Figure 1H).

(J) *Mz19-GAL4* driven *toll-6* expression in DA1, VA1d, and DC3 PNs fully rescues VA1d ORN axon mistargeting in *toll-6* mutants.

(K) Expression of Toll-6 in *Mz19-GAL4*$^{+}$ MARCM adNb clones, which include VA1d and DC3 PNs, rescues VA1d ORN axon mistargeting (labeled by *Or88a-rCD2* in green) in *toll-6* mutants.

(L) Quantification of VA1d ORN axon mistargeting in *toll-6* whole-animal mutants compared to rescue by expression of *toll-6* in *Mz19*$^{+}$ PNs or in adNb MARCM clones.

(expressed in PNs) and *D42-GAL4* recapitulated the original *D42-GAL4* expression pattern (Figure 4F). Intersection between *eyFLP* (expressed in ORNs) and *D42-GAL4* also resulted in strong expression in anterolateral glomeruli, consistent with the original D42 expression pattern (Figure 4G). Taken together, these experiments indicate Toll-6 is expressed in ORN axons and PN dendrites that target to largely overlapping glomeruli.

Since Toll-6 is expressed in both ORNs and PNs, we next asked whether Toll-6 acts in ORNs, PNs, or both for targeting to the VA1d glomerulus. VA1d ORN axon targeting was normal following *Pebbled-GAL4*-driven RNAi knockdown (Figure S1C) or *eyFLP* MARCM removal of *toll-6* from ORNs (Figure S1D), suggesting that Toll-6 is not required in ORNs. On the other hand, misexpression of *toll-6* in PNs with *Mz19-GAL4* fully rescued dorsal mistargeting of VA1d ORN axons (Figure 4J, compared to Figures 4I and 4L). Using *hsFLP* and heat shocking in newly hatched larvae to generate MARCM PN neuroblast clones (Jefferis et al., 2001), we further limited *Mz19-GAL4*-mediated expression of *toll-6* to VA1d and DC3 PNs in the anterodorsal neuroblast (adNb) lineage. Expression of *toll-6* in VA1d and DC3 PNs alone was sufficient to rescue VA1d ORN axon-targeting defects (Figures 4K and 4L). Consistently, RNAi removal of *toll-6* from PNs caused a low penetrance VA1d ORN axon mistargeting phenotype in 2 of 15 antennal lobes analyzed (data

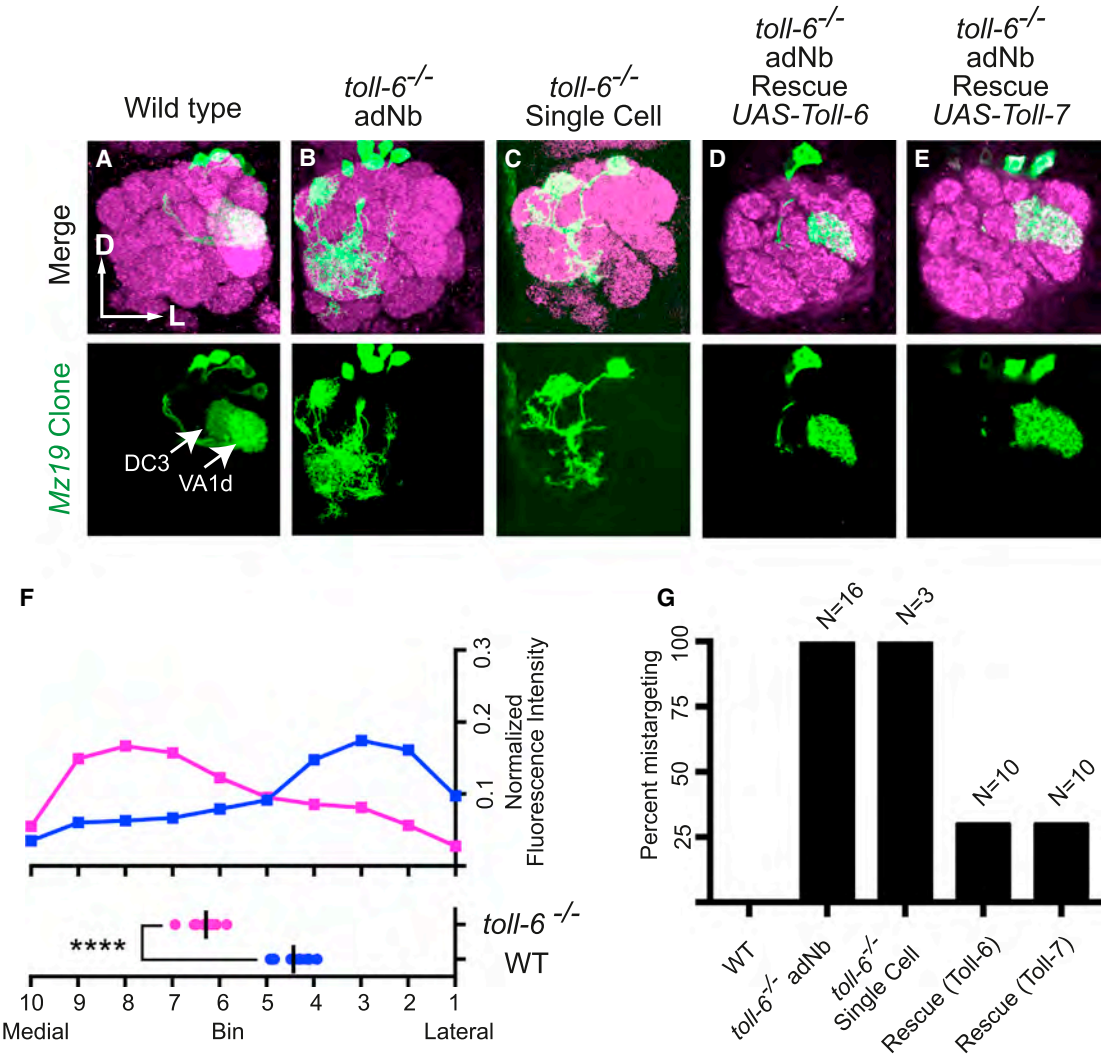


**Figure 5. Toll-6 Functions Cell Autonomously for PN Dendrite Targeting**

(A) *Mz19-GAL4*-labeled wild-type VA1d and DC3 PNs in adNb clones target dendrites to the VA1d and DC3 glomeruli in the lateral antennal lobe.

(B) *Mz19-GAL4*-labeled *toll-6*$^{-/-}$ VA1d and DC3 PNs in adNb clones mistarget dendrites to the medial antennal lobe.

(C) An *Mz19-GAL4*-labeled *toll-6*$^{-/-}$ VA1d (or DC3) single cell PN clone mistargets to the medial antennal lobe.

(D and E) PN dendrite targeting in *Mz19-GAL4*-labeled *toll-6*$^{-/-}$adNb clones is rescued by restricted misexpression of Toll-6 (D) or Toll-7 (E) only in these clones.

(F) Quantification of VA1d and DC3 PN dendrite mistargeting in *toll-6*$^{-/-}$ adNb clones, as in Figure 1I. VA1d and DC3 PN dendrite distribution (top) and mean intensity (bottom) are shifted medially in *toll-6* mutants.

(G) Quantification of VA1d and DC3 PN dendrite mistargeting in wild-type *Mz19*$^{+}$ adNb clones, *toll-6*$^{-/-}$ *Mz19-GAL4* adNb clones, *toll-6*$^{-/-}$ *Mz19-GAL4* single cell clones, and in *toll-6*$^{-/-}$ adNb clones in which *UAS-toll-6* or *UAS-toll-7* is misexpressed in the clones.

not shown). The low penetrance is possibly due to weak *GH146-GAL4* expression or perdurance of early expressed Toll-6 protein, yet it supports the notion that Toll-6 acts primarily in PNs for VA1d ORN axon targeting.

## Toll-6 Also Functions Cell Autonomously for PN Dendrite Targeting

In addition to being required for VA1d ORN axon targeting (Figures 4I–4K), we found that Toll-6 was also required in PNs for their dendrite targeting. In these experiments, we used *Mz19-GAL4*-based *hsFLP* MARCM to label *toll-6*$^{-/-}$ PN neuroblast clones, which normally target to the VA1d and DC3 glomeruli in the dorsolateral antennal lobe (Figure 5A). In *toll-6*$^{-/-}$ adNb clones, however, the VA1d and DC3 PN dendrites mistargeted extensively to dorsomedial and ventral positions in regions that normally did not express Toll-6 (Figures 5B and 5F). We further quantified fluorescence intensity of PN dendrites along the medial-lateral axis and found that removal of *toll-6* caused a significant medial PN dendritic shift compared with wild-type (Figure 5E). We also observed mistargeting of PN dendrites in single-cell MARCM clones of VA1d or DC3 PNs (Figures 5C and 5F). PN dendrite targeting

defects were rescued when we expressed a *UAS-toll-6* transgene in MARCM adNb clones (VA1d and DC3 PNs) that were *toll-6*$^{-/-}$ (Figures 5D and 5G). Together, these experiments indicate that Toll-6 is cell autonomously required in VA1d and DC3 PNs for dendrite targeting.

To explore the role of *toll-6* in dendrite targeting of other PN classes, we conducted *hsFLP*-based MARCM experiments and labeled with available PN-specific driver lines. We examined DA1 and VA1v PNs, which normally express Toll-6, as well as DM6 PNs, which do not express Toll-6. *toll-6*$^{-/-}$ DA1 PNs exhibited a low-penetrance localized medial dendrite mistargeting phenotype (Figure S4A), and *toll-6*$^{-/-}$ VA1v PNs displayed medial mistargeting of dendrites similar to the VA1d/DC3 defects (Figure S4B). Conversely, *toll-6*$^{-/-}$ DM6 PNs did not exhibit dendrite targeting defects (Figure S4C). Thus, Toll-6 is required for dendrite targeting in four classes of PNs that express Toll-6, but it is not required for dendrite targeting in one PN class that does not express Toll-6.

## Toll-6 and Toll-7 Play Instructive Roles in Target Selection

So far, we have shown that Toll-7 is cell autonomously required for axon targeting of specific ORN classes (Figure 3) and Toll-6 is cell autonomously required for dendrite targeting of specific PN classes (Figure 5). These ORN axons and PN dendrites target to Toll-7$^{+}$ (Figures 2A–2C) and Toll-6$^{+}$ (Figures 4A–4C) antennal lobe regions. These data suggest that Toll-7 and Toll-6 play instructive roles in ORN axon and PN dendrite targeting, respectively. To further test this idea, we performed the following gain-of-function experiments.

We first misexpressed *UAS-toll-7 in* two classes of ORNs, DM6 and DL4, during development using *Am29-GAL4* (Figure 6A). DM6 is normally located at the dorsomedial edge of the antennal lobe, outside the Toll-7$^{+}$ region (Figure 7A), but misexpression of *toll-7* caused a severe lateral mistargeting of DM6 ORN axons to the Toll-7$^{+}$ region (Figures 6B and 6L). DL4 ORN axons were unaffected, which may be explained by their proximity to, or inclusion within, the Toll-7$^{+}$ region. Thus, misexpression of Toll-7 caused the axons of a Toll-7-negative ORN class to mistarget to the Toll-7$^{+}$ region, supporting an instructive role of Toll-7 in ORN axon targeting.

In an analogous experiment, we misexpressed *UAS-toll-6* in VM6 PNs during development using the Janelia GAL4 line *71D09* (Jenett et al., 2012; B. Wu and L.L., unpublished data). VM6 is normally located at the posterior ventromedial edge of the antennal lobe (Figure 6E), outside the Toll-6$^{+}$ region. However, misexpression of Toll-6 in VM6 PNs caused an anterolateral shift in PN dendrite targeting, such that some VM6 PN dendrites mistargeted within the VA1v glomerulus (Figures 6F and 6M), which normally expresses Toll-6 (Figure 4A). Together, these data indicate that *toll-6* and *toll-7* act instructively in PNs and ORNs, respectively, for targeting their dendrites and axons to the Toll-6-/Toll-7-enriched region.

## Misexpressed Toll-6 and Toll-7 Appear to Function Equivalently

Given the different phenotypes and cell type specificities of these two highly related Toll receptors in olfactory circuit wiring, we next examined their molecular mechanisms. Blast comparison revealed that Toll-6 and Toll-7 proteins share 40% sequence identity, with similar domain organization (Figure 1J). Given these gross structural similarities, we asked whether Toll-6 and Toll-7 could replace each other's function. Using the *Am29-GAL4* misexpression assay, we found that Toll-6 misexpression in DM6 ORNs caused severe lateral mistargeting of ORN axons (Figures 6C and 6L), similar to Toll-7 misexpression (Figure 6B). Toll-2, Toll-6, Toll-7, and Toll-8 are closest among the 9 *Drosophila* Toll receptors and represent a subfamily based on alignment of the Toll-family cytosolic TIR-containing domains (Leulier and Lemaitre, 2008). Interestingly, *Am29-GAL4* misexpression of Toll-2 and Toll-8 also resulted in lateral targeting defects of DM6 ORN axons (data not shown) similar to Toll-6 and Toll-7 misexpression. By contrast, targeting of DM6 ORN axons was normal following *Am29-GAL4* misexpression of the other Toll-family members, including Toll-1, -3, -4, -5, and -9 (data not shown). Thus, only the Toll-2/6/7/8 subfamily members exhibited similar activity in this misexpression assay.

We also examined whether Toll-7 is capable of rescuing *toll-6* mutant ORN axon and PN dendrite targeting defects. Expression of *UAS-toll-7* using *Mz19-GAL4* rescued the VA1d ORN axon targeting defects seen in *toll-6* mutants (Figures 6K and 6N). Further, expression of *toll-7* in *toll-6*$^{-/-}$ *Mz19*$^{+}$ MARCM adNb PN clones (Figures 5E and 5G) rescued the severe PN dendrite targeting defects observed in *toll-6*$^{-/-}$ clones (Figure 5B). Thus, in addition to the equivalence in misexpression assays (Figures 6A–6C), Toll-7 can replace the olfactory wiring functions of Toll-6 in PNs during development.

## The Canonical Toll Signaling Pathway Is Not Required for VA1d ORN Axon Targeting

In the context of embryonic dorsal-ventral pattern formation and innate immune response, Toll-1 and Toll-like receptors (TLRs) function upstream of a conserved, canonical Toll-signaling cascade to activate NF-κB factors and regulate transcription (Imler and Zheng, 2004). To investigate whether Toll-6 and Toll-7 utilize canonical Toll signaling for olfactory circuit wiring, we examined the requirement of critical Toll pathway components, including the TIR adaptor protein dMyD88 and the two NF-κB factors Dorsal and Dif, using VA1d ORN axon targeting as an assay. VA1d ORN axon targeting was normal in two different *dMyD88* alleles, *dMyD88*$^{EP2133}$ and *dMyD88*$^{C03881}$, as well as in *dl*$^{1}$ and *Dif*$^{1}$ (Figures S6A–S6D). *Drosophila* Toll-1 is activated by its ligand Spätzle (Spz) (Imler and Zheng, 2004), and evidence suggests the Spz homologs DNT1 and DNT2 (also named Spz-2 and Spz-5, respectively) are ligands for Toll-6 and Toll-7 (McIlroy et al., 2013). VA1d ORN axon targeting was normal in two different Spz alleles (*spz*$^{2}$ and *spz*$^{3}$; data not shown). We also tested whether DNT1 and DNT2 are involved in olfactory circuit wiring specificity. *Mz19*$^{+}$ PN dendrites and VA1d ORN axons targeted normally in *dNT2*, *dNT1* double null mutant flies (Figure S6E). These findings indicate the canonical Toll-signaling cascade, from ligands to downstream signaling partners, is not required for VA1d ORN axon targeting.

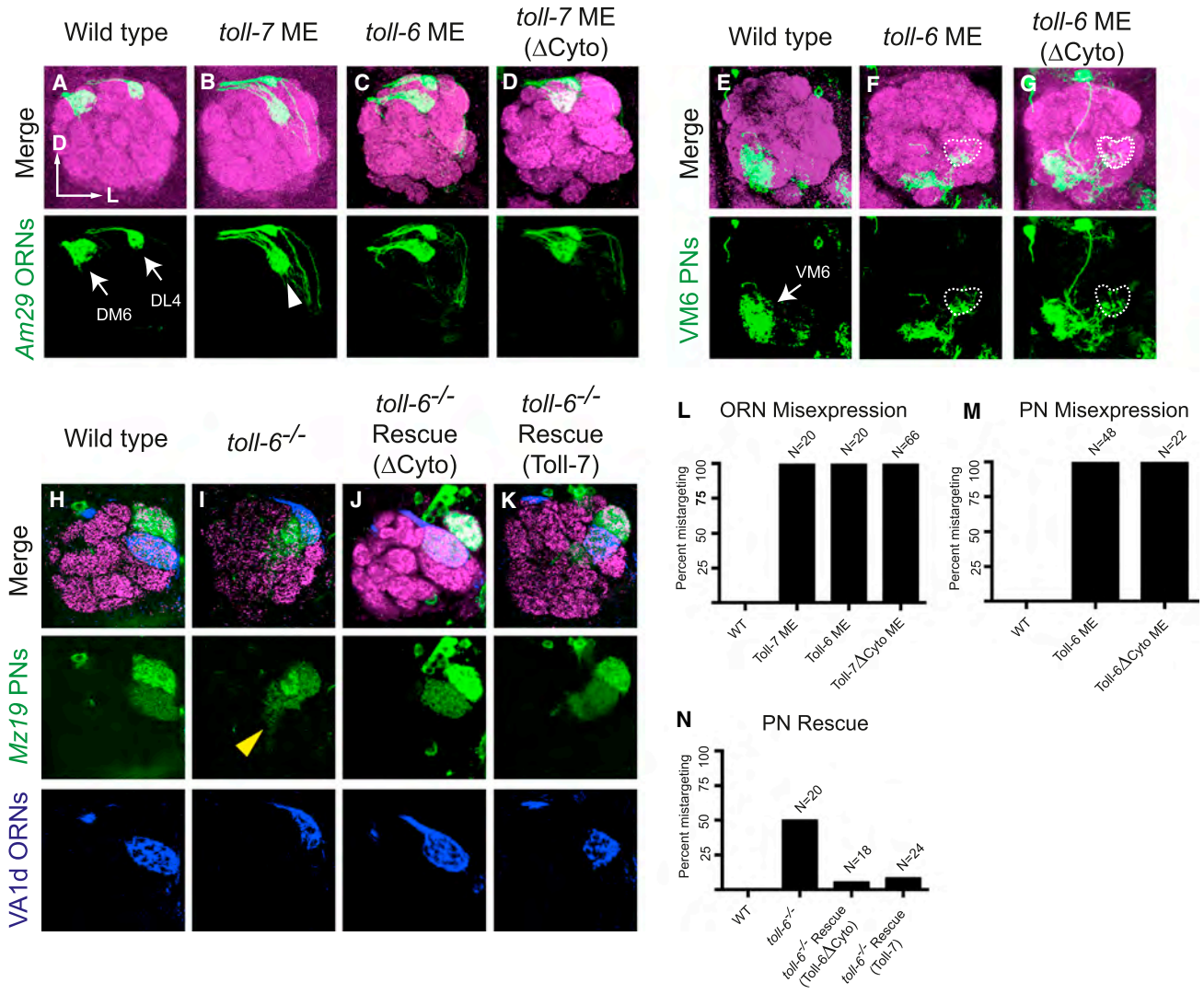


**Figure 6. Toll-6 and Toll-7 Play Instructive Roles in Target Selection, and Their Cytoplasmic Domains Are Dispensable**

All panels show labeling of specific PN and ORN classes and a merged image with neuropil labeling of the same single confocal section.

(A) In wild-type, *Am29-GAL4* labels ORN axons targeting to the DM6 and DL4 glomeruli (arrows) in the dorsomedial and dorsolateral antennal lobe, respectively.

(B) *Am29-GAL4* misexpression (ME) of Toll-7 causes lateral mistargeting of DM6 ORN axons to the Toll-7$^{+}$ region (white arrowhead). DL4 ORNs appear unperturbed.

(C) *Am29-GAL4* misexpression of Toll-6 also causes DM6 ORN axon mistargeting.

(D) Misexpression of a truncated Toll-7 in which the cytoplasmic domain is replaced with GFP recapitulates wild-type Toll-7 misexpression.

(E) In wild-type, *71D09-GAL4* labels dendrites of VM6 PNs (arrow) targeting the posterior ventromedial antennal lobe.

(F) *71D09-GAL4* misexpression of Toll-6 causes lateral mistargeting of VM6 PN dendrites to the Toll-6$^{+}$ region including the VA1v glomerulus (dashed line).

(G) Misexpression of a truncated Toll-6 transgene in which the cytoplasmic domain is replaced with GFP recapitulates wild-type Toll-6 misexpression.

(H) In wild-type control, dendrites of DA1 and VA1d PNs visualized by *Mz19-GAL4* (green) and VA1d ORNs labeled with *Or88a-myr-tdT* (pseudocolored blue) target to the lateral antennal lobe. *Mz19-GAL4* also labels dendrites of DC3 PNs, which are not in this confocal section.

(I) In *toll-6* mutants, VA1d ORN axons mistarget dorsally to a lateral position with respect to DA1. *Mz19-GAL4* PN dendrites mistarget (yellow arrowhead) diffusely in the antennal lobe and partially colocalize with mistargeted VA1d ORNs.

(J) Misexpression of a cytoplasmic domain truncated Toll-6 in PNs by *Mz19-GAL4* rescues VA1d ORN axon and PN dendrite targeting defects.

(K) Misexpression of Toll-7 in PNs by *Mz19-GAL4* also rescues VA1d ORN axon and PN dendrite targeting defects.

(L) Quantification of DM6 ORN axon targeting in wild-type and following *Am29-GAL4* misexpression of *UAS-toll-7*, *UAS-toll-6*, or *UAS-toll-7ΔCyto*.

(M) Quantification of VM6 PN dendrite mistargeting in wild-type and following *71D09-GAL4* misexpression of *UAS-toll-6* or *UAS-toll-6ΔCyto*.

(N) Quantification of VA1d ORN axon mistargeting in wild-type, *toll-6* mutants (same as Figure 1H), and in rescue experiments in which *UAS-toll-6ΔCyto* or *UAS-toll-7* is misexpressed in *Mz19-GAL4* labeled PNs in *toll-6* mutants.

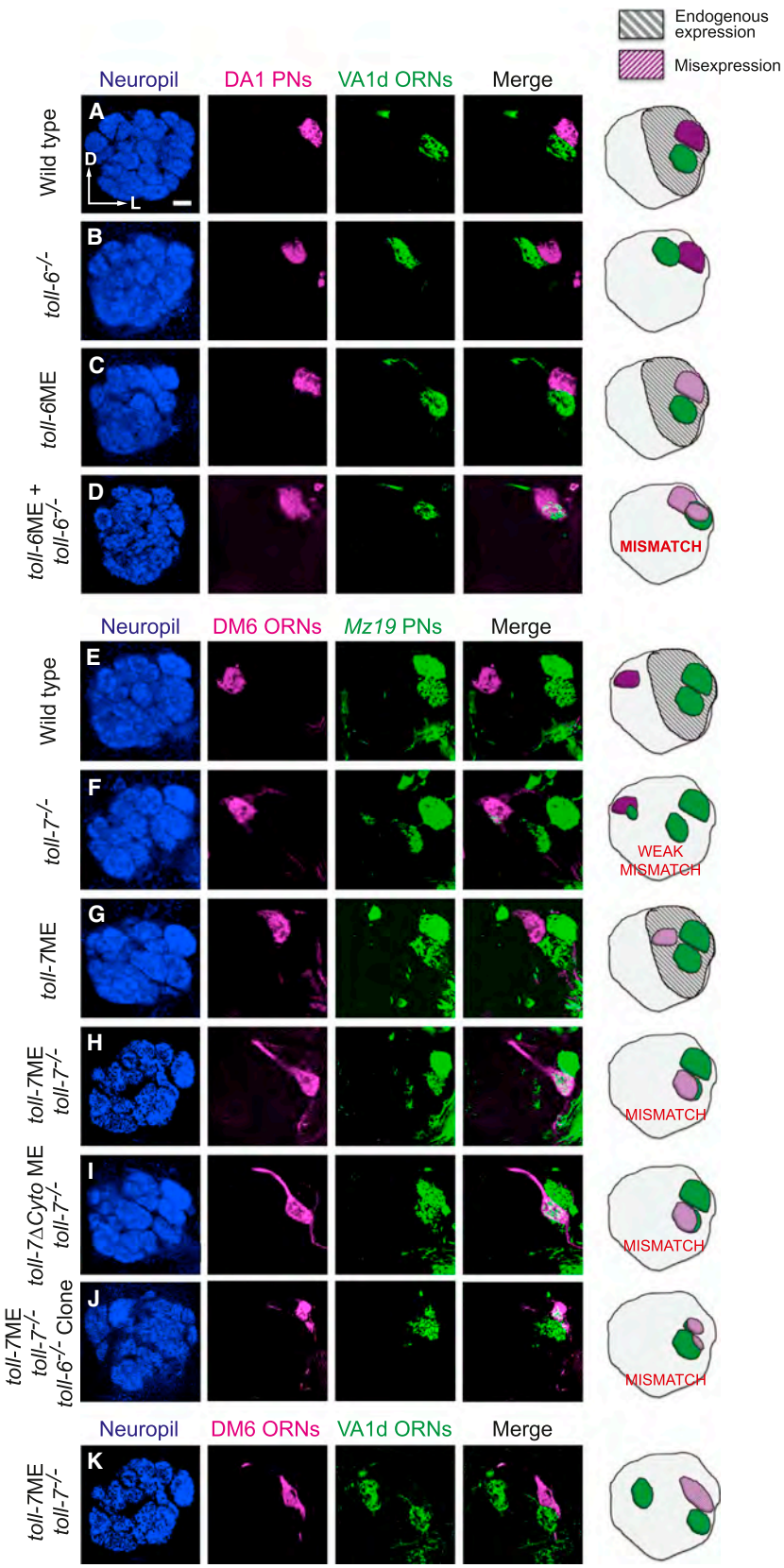


**Figure 7. Toll-6 and Toll-7 Mediate Synaptic Partner Matching**

Left panels are single-section confocal images stained with neuropil marker, PN dendrites, ORN axons, and their merge as indicated. The right panel shows the schematic interpretation. (A)–(D) test the role of Toll-6, and (E)–(K) test the role of Toll-7, in synaptic partner matching.

(A) In wild-type, axons of VA1d ORNs labeled with *Or88a-myr-tdT* (pseudocolored green) target to the VA1d glomerulus ventral to DA1. The DA1 glomerulus is labeled here by dendrites of DA1 PNs (magenta) visualized by *Mz19-GAL4*-based MARCM lateral neuroblast clones. No intermingling of VA1d ORN axons and DA1 PN dendrites results (scale bar is 10 μm).

(B) In *toll-6*$^{-/-}$ whole-animal mutants, VA1d ORN axons mistarget dorsally (see also Figure 1F). No intermingling of VA1d ORN axons and DA1 PN dendrites results (0/10 mismatch).

(C) When Toll-6 is misexpressed in DA1 PNs in *Mz19-GAL4*-based MARCM lateral neuroblast clones in an otherwise wild-type background, no intermingling of VA1d ORN axons and DA1 PN dendrites results (0/10 mismatch).

(D) When Toll-6 is misexpressed in DA1 PNs in *Mz19-GAL4*-based MARCM lateral neuroblast clones in *toll-6*$^{-/-}$ whole-animal mutants, extensive intermingling of VA1d ORN axons and DA1 PN dendrites occurs (13/15 mismatch).

(E) In wild-type, *Am29-GAL4* labels axons of DM6 ORN axons targeting the dorsomedial antennal lobe (it also labels ORN axons targeting the DL4 glomerulus, which is in a more posterior confocal plane and thus is not visible). *Mz19-QF* labels dendrites of DA1 and VA1d PNs in the lateral antennal lobe, far away from DM6 ORN axons.

(F) In *toll-7* whole-animal mutants, a subset of VA1d PN dendrites mistarget medially, following the mistargeted VA1d ORNs, some of which mismatch with DM6 ORNs in the vicinity (3/10 antennal lobes exhibit mismatching of comparable severity to this example).

(G) Misexpressing Toll-7 with *AM29-GAL4* in an otherwise wild-type background causes DM6 ORN axons to mistarget laterally (similar to Figure 6B) to a Toll-7$^{+}$ area, adjacent to Mz-19$^{+}$ dendrites, but does not result in intermingling with Mz-19$^{+}$ PN dendrites (0/8 mismatch).

(H) When Toll-7 is misexpressed with *AM29-GAL4* in a *toll-7* whole-animal mutant background, laterally mistargeted DM6 ORN axons extensively intermingle with *Mz19*$^{+}$ PN dendrites (31/38 antennal lobes exhibit mismatching of comparable severity to this example).

(I) Misexpressing a truncated Toll-7 lacking its cytoplasmic domain (Toll-7ΔCyto) with *AM29-GAL4* in a *toll-7* whole-animal mutant background gives a similar mismatching phenotype as misexpressing wild-type Toll-7 in panel H (6/6 antennal lobes mismatch with a comparable severity to this example).

(J) The DM6 ORN axons and VA1d PN dendrites still mismatch when Toll-7 is misexpressed with *AM29-GAL4* in a *toll-7* whole-animal mutant background following *Mz19* Q-MARCM removal of *toll-6* from adNb clones (4/7 antennal lobes mismatch with a comparable severity to this example).

(K) When Toll-7 is misexpressed by *AM29-GAL4* in a *toll-7* whole-animal mutant background, laterally mistargeted DM6 ORN axons do not comingle with VA1d ORN axons (0/30 antennal lobes display DM6 and VA1d ORN axon comingling).

### The Cytosolic Domains of Toll-6 and Toll-7 Are Dispensable for Olfactory Circuit Wiring

To further examine the signaling mechanisms of Toll-6 and Toll-7 in olfactory circuit wiring, in particular whether signaling through the conserved Toll-6 and Toll-7 TIR domains is required, we made *UAS*-transgenes in which two critical TIR domain residues (Ohnishi et al., 2009; Xu et al., 2000) were mutated (TIR-dead). We also replaced the entire cytosolic domain by GFP (ΔCyto). Surprisingly, *Am29-GAL4*-driven misexpression of *UAS-toll-7$^{TIR\text{-}dead}$* (Figure S5A) and *UAS-toll-7$^{\Delta Cyto}$* (Figures 6D and 6L) resulted in lateral mistargeting of DM6 ORN axons, a phenotype indistinguishable from misexpressing the wild-type *UAS-toll-7* transgene (Figure 6B). In addition, *71D09-GAL4*-driven misexpression of *UAS-toll-6$^{\Delta Cyto}$* caused lateral mistargeting of VM6 PN dendrites (Figures 6G and 6M). Thus, the cytosolic domains of Toll-6 and Toll-7 are dispensable for their gain-of-function effects on PN dendrite and ORN axon targeting, respectively.

To test whether the TIR/cytosolic domains are required for rescue of VA1d PN and ORN phenotypes observed in *toll-6* mutants, we used *Mz19-GAL4* to express the mutant transgenes in DA1, VA1d, and DC3 PNs. We found that *UAS-toll-6$^{TIR\text{-}dead}$* (Figure S5B) and *UAS-toll-6$^{\Delta Cyto}$* (Figures 6H–6J and 6N) rescued both ORN axon- and PN dendrite-targeting phenotypes, indicating that the functions of Toll-6 and Toll-7 in olfactory wiring do not depend on the intracellular signaling capacities of these proteins.

### Toll-6 and Toll-7 Mediate Synaptic Partner Matching Using Heterophilic Molecular Partners

Lastly, we describe a set of experiments that shed light on the cellular mechanisms by which Toll receptors regulate olfactory system wiring specificity. VA1d ORN axons and DA1 PN dendrites normally targeted to adjacent glomeruli and never mismatched in wild-type animals (Figure 7A). However, under the condition where all cells lacked endogenous Toll-6 and DA1 PNs expressed Toll-6 from a transgene (in *Mz19-GAL4*-based MARCM lateral neuroblast clones), there was a strong mismatch between VA1d ORN axons and DA1 PN dendrites (Figure 7D). This mismatching did not occur either when all cells lacked Toll-6 alone (Figure 7B) or when DA1 PNs expressed Toll-6 from a transgene in an otherwise wild-type background (Figure 7C).

Given the cell-autonomous function of Toll-6 in PN dendrite targeting (Figure 5), and that expressing Toll-6 in PNs can rescue ORN axon mistargeting phenotypes in *toll-6* whole-animal mutants (Figure 4), the simplest model that can explain the mismatching phenotypes is that, in addition to regulating PN dendrite targeting, Toll-6 in PNs also regulates ORN–PN partner matching with its cognate ORN partners. Adding Toll-6 back only in DA1 PNs in a whole-animal mutant background makes DA1 PN dendrites the preferred PN partner for VA1d ORN axons. We have previously identified two Teneurins, Ten-m and Ten-a, as homophilic partner matching molecules that differ in their expression between VA1d and DA1 and contribute to the ORN-PN partner matching of these glomeruli (Hong et al., 2012). The fact that manipulation of *toll-6* alone is capable of causing mismatching of DA1 PN dendrites and VA1d ORN axons suggests Toll-6 is a potent partner-matching factor that can override other matching mechanisms. That mismatching occurred between Toll-6-expressing DA1 PN dendrites and Toll-6-lacking VA1d ORN axons suggests that Toll-6 interacts with a heterophilic ligand for partner matching.

Next, we designed a similar set of experiments to explore whether Toll-7 could have an analogous role in synaptic partner matching, this time between Toll-7-expressing ORN axons and their cognate PN dendrites. As shown earlier, misexpression of Toll-7 in DM6 ORNs using *Am29-GAL4* caused a lateral mistargeting of DM6 ORN axons (Figure 6B). When we co-labeled *Mz19*$^{+}$ PNs in the same animal, we found that Toll-7-misexpressing DM6 ORN axons mistargeted to an antennal lobe position just medial to the VA1d glomerulus but did not intermingle with *Mz19*$^{+}$ PN dendrites (Figure 7G, compared to control in Figure 7E). However, when we performed the same misexpression experiments in the *toll-7* whole-animal mutant background, we observed extensive mismatching between DM6 ORN axons and *Mz19*$^{+}$ PN dendrites—most likely VA1d dendrites as judged from the location (Figure 7H). To test whether this Toll-7-mediated mismatching phenotype is dependent on the activity of Toll-6 in PNs, we used Q-MARCM (Potter et al., 2010) to remove *toll-6* from *Mz19*$^{+}$ MARCM adNb clones in a *toll-7* mutant background while simultaneously misexpressing Toll-7 in DM6 ORNs (Figure 7J). We still observed mismatching between DM6 ORNs and the *toll-6*$^{-/-}$ clones, suggesting Toll-6 is not a ligand for Toll-7 in this matching experiment.

The mismatching between DM6 ORNs and *Mz19*$^{+}$ PN dendrites could be due to (1) direct mismatching between ORNs and PNs or (2) failed segregation between DM6 and VA1d ORN axons, and as a secondary consequence DM6 ORNs mismatched with VA1d PNs. To distinguish between these two possibilities, we differentially labeled DM6 and VA1d ORNs in the above mismatching experiment and observed that DM6 and VA1d ORN axons remained segregated (Figure 7K). This strongly suggests that the overlap between DM6 ORN axons with *Mz19*$^{+}$ PN dendrites in experiments shown in Figure 7H resulted from direct mismatching between ORN axons and PN dendrites, as opposed to failed segregation between DM6 and VA1d ORN axons. Moreover, in *toll-7* mutants we occasionally observed minor mismatching phenotypes between DM6 ORN axons and mistargeted VA1d PN dendrites (Figure 7F), indicating that these classes are partially competent to match. As shown previously, PNs labeled by *Mz19-GAL4* elaborate dendrites that partially overlap with ORN axons of non-matching classes during early stages of olfactory circuit development (Figure S2). Thus, olfactory wiring appears to be a dynamic process subject to global mismatching events, such as in cases when the partner matching cell surface code is altered (Figure 7H).

Finally, we tested whether Toll-7 signaling through its cytoplasmic domain is required for these mismatching phenotypes. We found that *AM29-GAL4*-driven misexpression of *UAS-toll-7$^{\Delta Cyto}$* in the *toll-7* mutant background recapitulated the mismatching phenotypes (Figure 7I), indicating that signaling through the cytoplasmic domain of Toll-7 is not required for its synaptic partner matching function.

## DISCUSSION

Our high-resolution confocal-based screen of transmembrane and secreted proteins identified two Toll-family receptors that regulate different aspects of olfactory circuit wiring (Figure 1). Toll-7 is expressed in ORN axons that target to a cluster of anterolateral glomeruli (Figure 2) and functions cell autonomously in VA1d and DA1 ORNs for their axon targeting (Figure 3). Toll-6 is localized to a similar cluster of anterolateral glomeruli but is expressed from both ORNs and PNs (Figure 4). Toll-6 cell autonomously regulates PN dendrite targeting (Figure 5), and Toll-6 in PNs is sufficient to regulate ORN axon targeting (Figure 4). Misexpression studies indicate that Toll-6 and Toll-7 instruct PN dendrite and ORN axon targeting, respectively. Both Toll-6 and Toll-7 also participate in partner matching of the VA1d glomerulus (Figure 7), with Toll-6 functioning in PNs and Toll-7 in ORNs. This raises the intriguing idea that partner matching may be part of a larger dynamic strategy of PN dendrite and ORN axon target selection. The activities of Toll-6 and Toll-7 in olfactory circuit wiring do not require their cytoplasmic domains or their canonical signaling pathway members (Figure 6), suggesting the involvement of signaling pathways with a novel ligand(s) and co-receptor(s).

### Toll-6 and Toll-7 Instruct Olfactory Circuit Assembly via a Non-canonical Mechanism

Toll-family receptors are best known for their functions in innate immunity and also have important roles in development, including embryonic patterning, and in tissue morphogenesis (Imler and Zheng, 2004; Paré et al., 2014). In addition, Toll-1, Toll-6, Toll-7, and Toll-8 have been implicated in regulating embryonic motor axon targeting (McIlroy et al., 2013; Rose et al., 1997) and synaptic growth at the neuromuscular junction (Ballard et al., 2014). Vertebrate TLRs regulate hippocampal neurogenesis in adult mice (Rolls et al., 2007) and promote dendrite outgrowth in vitro (Liu et al., 2013; Ma et al., 2006). However, neurodevelopmental defects have so far not been observed in mouse TLR knockouts, which could be due to redundancy in the TLR family.

Our study identified a role for Toll-family receptors in wiring specificity of neural circuits in the brain. Surprisingly, the activation and signaling mechanisms of Toll-6 and Toll-7 are non-canonical, in contrast to a previous report based on in vitro assays (McIlroy et al., 2013). In *Drosophila*, the embryonic patterning and immune functions of Toll-1 are activated in response to its ligand Spz, resulting in signaling through NF-κB members Dorsal and Dif, respectively. At the neuromuscular junction, the Spz homologs DNT2 and DNT1 have been proposed to serve as ligands for Toll-6 and Toll-7, and evidence suggests that Toll-6 and Toll-7 signal through a canonical NF-κB pathway (McIlroy et al., 2013). We found that targeting of VA1d PN dendrites and ORN axons was normal in *dNT2*, *dNT1* double null mutants (Figure S6E), indicating that Toll-6 and Toll-7 do not use the DNT1/2 ligands in the context of olfactory circuit wiring. Previous work has also shown that Toll receptors promote cell aggregation in in vitro S2 cell assays (Keith and Gay, 1990; Paré et al., 2014). We did not observe homophilic or heterophilic interaction of Toll-6 and Toll-7 in S2 cell aggregation assays (data not shown). Thus, Toll-6 and Toll-7 do not appear to function as homophilic or heterophilic ligand-receptor pairs. Indeed, our findings suggest Toll-6 and Toll-7 interact with a heterophilic partner(s) in synaptic partner matching functions (Figure 7). The distinct *toll-6* and *toll-7* mutant phenotypes (Figure 1) and the Toll-7-mediated mismatching observed with *toll-6*$^{-/-}$ PN clones (Figure 7J) argue against the possibility that they are a receptor-ligand pair. Lastly, we found the cytoplasmic domains of Toll-6 and Toll-7 to be dispensable for their activities in PNs and ORNs, respectively, suggesting that these receptors signal through a non-canonical co-receptor mechanism.

In summary, our studies identified essential functions of Toll receptors in regulating wiring specificity of the olfactory circuit. Our in vivo analyses suggest that Toll receptor signaling in olfactory circuit assembly differs from early development or innate immunity. These data imply the existence of novel Toll-6/7 ligands and co-receptors that mediate their function in wiring specificity. Future identification of these proteins will broaden our knowledge of Toll receptor function and shed further light on the molecular mechanisms that establish wiring specificity of neural circuits.

### Families of Wiring Specificity Molecules in Neural Circuit Assembly

Toll-6 and Toll-7 regulate reciprocal biological functions in PNs and ORNs, respectively. While Toll-6 functions in PNs and Toll-7 in ORNs, they each regulate targeting and matching of neuronal processes to the VA1d glomerulus. Interestingly, we found that all four members of the subfamily to which Toll-6 and Toll-7 belong have similar misexpression phenotypes in ORNs and that Toll-6 and Toll-7 are functionally equivalent for rescuing *toll-6* mutant VA1d PN dendrite- and ORN axon-targeting defects. Thus, the Toll-2/6/7/8 subfamily members exhibit similar functional properties in olfactory neuron wiring in the context of misexpression.

*Drosophila* Robo receptors are a well-characterized family of receptors that regulate different wiring decisions in longitudinal axon pathway choice in the embryonic CNS (Rajagopalan et al., 2000; Simpson et al., 2000). Robo1, Robo2, and Robo3 establish a combinatorial code for axon pathway selection in response to the midline repellent ligand Slit. The Robo swap experiments showed that pathway choice specificity was not dependent on the functional differences of Robo receptor proteins, but on their different spatiotemporal expression patterns (Spitzweck et al., 2010). Our finding of the functional equivalence of Toll-6 and Toll-7 in olfactory wiring when misexpressed resembles the Robo code: the distinct spatial expression pattern of a particular Toll receptor, rather than its unique structural facets, can determine its biological function. The fact that Toll-2 and Toll-8 have activities similar to Toll-6 and Toll-7 when misexpressed suggests that Toll-2 and Toll-8 could play analogous functions in wiring specificity in other parts of the nervous system, including classes of olfactory neurons not examined in this study. Toll-6 and Toll-7 receptors, and possibly other Toll receptors, may share a common ligand, co-receptor, or both, making them wiring specificity molecules whose spatiotemporal expression patterns can evolve to play distinct roles in wiring of the complex CNS circuits.

Our data also suggest that Toll-6 and Toll-7 do not play completely identical, redundant functions. For instance, our expression study indicates that VA1d ORNs express both Toll-6 and Toll-7 (Figures 2 and 4). Yet whole-animal or ORN-specific removal of Toll-7 is sufficient to produce VA1d ORN axon-targeting defects (Figures 1 and 2). This may be accounted for by differences in Toll-6 and Toll-7 temporal patterns of expression, different levels of expression, or their differential affinity for the ligand(s) or co-receptor(s).

In the *Drosophila* antennal lobe, thousands of neurons belonging to over 100 different classes extend axons and dendrites within a small, compact space, making specific choices during targeting to specific stereotyped positions. This process requires a large number of cell surface recognition molecules to bring axons and dendrites of the same neuronal class together and separate axons and dendrites from different classes. A certain level of redundancy could make the wiring process more robust (i.e., more resistant to perturbations of individual molecules), thus requiring a greater number of identity recognition molecules than the theoretical minimum (Hong and Luo, 2014). In principle, expressing multiple molecules such as Toll receptors in distinct spatiotemporal patterns and levels (or having distinct ligand-receptor affinities) can increase the capacity for a limited number of molecules to encode different neuronal identities, providing each class of olfactory neuron with a unique, partially redundant combination of recognition molecules.

### Long-Range Mismatching Phenotypes Suggest a Dynamic Wiring Process

Teneurins were previously identified to be essential for synaptic partner matching between PN dendrites and ORN axons, wherein loss-of-function and misexpression perturbations cause neighboring classes of PN dendrites and ORN axons to form ectopic connections (Hong et al., 2012). This mismatching appears local, as the mismatched glomeruli are located adjacently within the same region of the antennal lobe. Given that there are 50 pairs of PNs and ORNs, two Teneurins are clearly not the only molecules involved in synaptic partner matching. Indeed, we observed ectopic connections between DA1 PN dendrites with VA1d ORN axons following misexpression of *toll-6* in DA1 PNs in the whole-animal *toll-6* mutant background (Figure 7D). This mismatching also occurs locally, qualitatively similar to what we observed with Teneurin perturbations. Surprisingly, we also observed mismatching between DM6 ORN axons and VA1d PN dendrites when misexpressing Toll-7 in DM6 ORNs in the whole-animal *toll-7* mutant background (Figure 7H). This is unexpected considering that DM6 ORN axons and VA1d PN dendrites normally target to the medial and lateral edge of the antennal lobe, respectively; in this complex genetic manipulation, they mismatch across the entire antennal lobe, which we term "global mismatching."

Previous work showed that PNs target their dendrites to approximate regions of the antennal lobe that correspond to their final glomerular position, before the arrival of pioneering ORN axons (Jefferis et al., 2004; Komiyama et al., 2007). This suggests a model whereby PN dendrites pre-pattern the antennal lobe, serving as a relatively fixed target for projecting ORN axons to partner with, and therefore matching would be a local mechanism segregating neighboring glomeruli. Here, the Toll-7 findings serve as the first example of a global mismatching between glomeruli that are at much greater distance. This suggests PN dendrites are more dynamic and are capable of sampling a relatively large portion of the antennal lobe during ORN axon invasion. Additionally, synaptic partner matching between PN dendrites and ORN axons may begin at an early stage before confinement of PN dendrites to their final target area (Figure S2). Together, these data suggest that PN dendrite and ORN axon targeting is more dynamic than previously appreciated. As a result, synaptic partner sampling would occur on a larger, more global scale and may serve as an additional strategy for axon and dendrite targeting. In this view, the dynamic interplay of both PN dendrites and ORN axons is pivotal for final target selection, emphasizing the need for multiple partner matching molecules, such as Tolls and Teneurins, to prevent not only local, but also global, mismatching.

## EXPERIMENTAL PROCEDURES

See Supplemental Experimental Procedures for detailed descriptions of mutants and transgenes used in this study.

### RNAi Screening

The RNAi screen fly was generated as follows: *C155-GAL4* was recombined with *UAS-dcr2* on the X chromosome. *Mz19-QF* was recombined with *QUAS-mCD8GFP*, *Or88a-Myr-tdTomato*, and *Or47b-ratCD2* on the second chromosome. These flies were crossed together to make a stable RNAi screen stock. Virgin females were collected from the RNAi screen stock and crossed to *UAS-RNAi* males. Females were allowed to lay eggs for 2 days at 25°C then shifted to 29°C to enhance the GAL4/UAS expression system. Progeny were collected within 2 days of eclosion, and the brains were dissected and fixed. We tested between two to three independent RNAi lines (different hairpins) per gene. For each RNAi line tested, 12 brains were dissected, fixed and immunostained, and of these, at least three were imaged by confocal microscopy.

### Mosaic Analysis

*hsFlp* MARCM analyses were performed as previously described (Jefferis et al., 2001; Komiyama et al., 2004; Lee and Luo, 1999). In summary, for adNb and lNb clones, flies were heat shocked for 1 hr at 37°C between 2 and 26 hr after larval hatching. To analyze ORN axon projections in adult brains using *hsFlp* MARCM, animals between 0–24 hr APF were heat shocked for 1 hr at 37°C. *eyFLP* MARCM and reverse MARCM was performed as described previously (Zhu and Luo, 2004).

### Immunostaining

Tissue dissection and immunostaining were performed according to previously described methods (Sweeney et al., 2007). Rat anti-Toll-6 antibody was custom produced by Thermo Scientific Pierce against a peptide epitope containing Toll-6 residues 62 to 81 (RPLTAGAGGDPSLYDAPDDC). Rabbit anti-Toll-7 antibody was custom produced by YenZym against Toll-7 residues 1,425 to 1,442 (QQPNPTAVSGQQQGPHVQ). Commercially available antibodies used in these studies include mouse nc82 (1:35; Developmental Studies Hybridoma Bank, [DSHB]), rat anti-DNcad (DN-Ex #8; 1:40; DSHB), chicken anti-GFP (1:1000; Aves Labs), rabbit anti-DsRed (1:250; Clontech), and mouse anti-ratCD2 (OX-34; 1:200; AbD Serotec). Secondary antibodies were raised in goat or donkey against rabbit, mouse, rat, and chicken antisera (Jackson Immunoresearch), conjugated to Alexa 405, 488, FITC, Cy3, Cy5, or Alexa 647.

### Imaging and Quantification Procedure

Confocal images were collected with a Zeiss LSM 510 or LSM 780 and processed with ImageJ and Adobe Photoshop. For assessment of *toll-7* mutant ORN axon and *toll-6* mutant PN dendrite targeting defects, the relative

fluorescence intensity was quantified by binning along the lateral-medial axis using MATLAB as described previously (Komiyama et al., 2007). Quantification of the *toll-6* mutant ORN axon targeting phenotype was scored by the experimenter according to position of VA1d ORN axons relative to the DA1 glomerulus (i.e., ventral, dorsomedial, or dorsolateral) per antennal lobe. Mistargeting frequency was calculated as (hemispheres with mistargeting)/(total brain hemispheres). Graphs were generated using the GraphPad Prism software.

## SUPPLEMENTAL INFORMATION

Supplemental Information includes six figures and Supplemental Experimental Procedures and can be found with this article online at http://dx.doi.org/10.1016/j.neuron.2015.02.003.

## AUTHOR CONTRIBUTIONS

A.W., H.W., and L.L. designed the study. A.W. and H.W. performed the RNAi screen and initial phenotypic analysis. A.W. completed the rest of the experiments with contribution from V.F. A.W. wrote the manuscript with substantial contribution from H.W. and L.L. L.L. supervised the project.

## ACKNOWLEDGMENTS

We thank D. Luginbuhl for technical assistance, B. Wu and H. Zhu for sharing unpublished results, the TRiP at Harvard Medical School (NIH/NIGMS R01-GM084947) and the VDRC for providing transgenic RNAi fly stocks, the Bloomington Stock Center for mutant alleles and transgenic flies, the Kyoto DGRC for NP lines, S. Cherry and J.M. Reichhart for *dMyD88* alleles, A. Hidalgo for the *dNT1* allele, T. Lee and G. Rubin for *71D09-GAL4*, and T. Clandinin for 853-GAL4. We thank K. Beier, L. DeNardo, X. Gao, C. Guenthner, T. Mosca, B. Wu, Xin Wang, and Xiang Wang for discussion and critiques on the manuscript. A.W. is a Damon Runyon HHMI fellow supported by the Damon Runyon Cancer Research Foundation (DRG-2098-11). L.L. is an investigator of the Howard Hughes Medical Institute. This work was supported by an NIH grant (R01-DC005982 to L.L.).

Received: October 2, 2014
Revised: December 26, 2014
Accepted: January 23, 2015
Published: March 4, 2015

## REFERENCES

Ballard, S.L., Miller, D.L., and Ganetzky, B. (2014). Retrograde neurotrophin signaling through Tollo regulates synaptic growth in Drosophila. J. Cell Biol. *204*, 1157–1172.

Chia, P.H., Li, P., and Shen, K. (2013). Cell biology in neuroscience: cellular and molecular mechanisms underlying presynapse formation. J. Cell Biol. *203*, 11–22.

Chou, Y.H., Zheng, X., Beachy, P.A., and Luo, L. (2010). Patterning axon targeting of olfactory receptor neurons by coupled hedgehog signaling at two distinct steps. Cell *142*, 954–966.

Couto, A., Alenius, M., and Dickson, B.J. (2005). Molecular, anatomical, and functional organization of the Drosophila olfactory system. Curr. Biol. *15*, 1535–1547.

Endo, K., Aoki, T., Yoda, Y., Kimura, K., and Hama, C. (2007). Notch signal organizes the Drosophila olfactory circuitry by diversifying the sensory neuronal lineages. Nat. Neurosci. *10*, 153–160.

Fishilevich, E., and Vosshall, L.B. (2005). Genetic and functional subdivision of the Drosophila antennal lobe. Curr. Biol. *15*, 1548–1553.

Hong, W., and Luo, L. (2014). Genetic control of wiring specificity in the fly olfactory system. Genetics *196*, 17–29.

Hong, W., Zhu, H., Potter, C.J., Barsh, G., Kurusu, M., Zinn, K., and Luo, L. (2009). Leucine-rich repeat transmembrane proteins instruct discrete dendrite targeting in an olfactory map. Nat. Neurosci. *12*, 1542–1550.

Hong, W., Mosca, T.J., and Luo, L. (2012). Teneurins instruct synaptic partner matching in an olfactory map. Nature *484*, 201–207.

Hummel, T., Vasconcelos, M.L., Clemens, J.C., Fishilevich, Y., Vosshall, L.B., and Zipursky, S.L. (2003). Axonal targeting of olfactory receptor neurons in Drosophila is controlled by Dscam. Neuron *37*, 221–231.

Imler, J.L., and Zheng, L. (2004). Biology of Toll receptors: lessons from insects and mammals. J. Leukoc. Biol. *75*, 18–26.

Jefferis, G.S., Marin, E.C., Stocker, R.F., and Luo, L. (2001). Target neuron prespecification in the olfactory map of Drosophila. Nature *414*, 204–208.

Jefferis, G.S., Vyas, R.M., Berdnik, D., Ramaekers, A., Stocker, R.F., Tanaka, N.K., Ito, K., and Luo, L. (2004). Developmental origin of wiring specificity in the olfactory system of Drosophila. Development *131*, 117–130.

Jenett, A., Rubin, G.M., Ngo, T.T., Shepherd, D., Murphy, C., Dionne, H., Pfeiffer, B.D., Cavallaro, A., Hall, D., Jeter, J., et al. (2012). A GAL4-driver line resource for *Drosophila* neurobiology. Cell Rep. *2*, 991–1001.

Joo, W.J., Sweeney, L.B., Liang, L., and Luo, L. (2013). Linking cell fate, trajectory choice, and target selection: genetic analysis of Sema-2b in olfactory axon targeting. Neuron *78*, 673–686.

Keith, F.J., and Gay, N.J. (1990). The Drosophila membrane receptor Toll can function to promote cellular adhesion. EMBO J. *9*, 4299–4306.

Kolodkin, A.L., and Tessier-Lavigne, M. (2011). Mechanisms and molecules of neuronal wiring: a primer. Cold Spring Harb. Perspect. Biol. *3*, http://dx.doi.org/10.1101/cshperspect.a001727.

Komiyama, T., Carlson, J.R., and Luo, L. (2004). Olfactory receptor neuron axon targeting: intrinsic transcriptional control and hierarchical interactions. Nat. Neurosci. *7*, 819–825.

Komiyama, T., Sweeney, L.B., Schuldiner, O., Garcia, K.C., and Luo, L. (2007). Graded expression of semaphorin-1a cell-autonomously directs dendritic targeting of olfactory projection neurons. Cell *128*, 399–410.

Kurusu, M., Cording, A., Taniguchi, M., Menon, K., Suzuki, E., and Zinn, K. (2008). A screen of cell-surface molecules identifies leucine-rich repeat proteins as key mediators of synaptic target selection. Neuron *59*, 972–985.

Lattemann, M., Zierau, A., Schulte, C., Seidl, S., Kuhlmann, B., and Hummel, T. (2007). Semaphorin-1a controls receptor neuron-specific axonal convergence in the primary olfactory center of Drosophila. Neuron *53*, 169–184.

Lee, T., and Luo, L. (1999). Mosaic analysis with a repressible cell marker for studies of gene function in neuronal morphogenesis. Neuron *22*, 451–461.

Leulier, F., and Lemaitre, B. (2008). Toll-like receptors—taking an evolutionary approach. Nat. Rev. Genet. *9*, 165–178.

Liu, H.Y., Hong, Y.F., Huang, C.M., Chen, C.Y., Huang, T.N., and Hsueh, Y.P. (2013). TLR7 negatively regulates dendrite outgrowth through the Myd88-c-Fos-IL-6 pathway. J. Neurosci. *33*, 11479–11493.

Luo, L., and Flanagan, J.G. (2007). Development of continuous and discrete neural maps. Neuron *56*, 284–300.

Ma, Y., Li, J., Chiu, I., Wang, Y., Sloane, J.A., Lü, J., Kosaras, B., Sidman, R.L., Volpe, J.J., and Vartanian, T. (2006). Toll-like receptor 8 functions as a negative regulator of neurite outgrowth and inducer of neuronal apoptosis. J. Cell Biol. *175*, 209–215.

McIlroy, G., Foldi, I., Aurikko, J., Wentzell, J.S., Lim, M.A., Fenton, J.C., Gay, N.J., and Hidalgo, A. (2013). Toll-6 and Toll-7 function as neurotrophin receptors in the Drosophila melanogaster CNS. Nat. Neurosci. *16*, 1248–1256.

Ohnishi, H., Tochio, H., Kato, Z., Orii, K.E., Li, A., Kimura, T., Hiroaki, H., Kondo, N., and Shirakawa, M. (2009). Structural basis for the multiple interactions of the MyD88 TIR domain in TLR4 signaling. Proc. Natl. Acad. Sci. USA *106*, 10260–10265.

Paré, A.C., Vichas, A., Fincher, C.T., Mirman, Z., Farrell, D.L., Mainieri, A., and Zallen, J.A. (2014). A positional Toll receptor code directs convergent extension in Drosophila. Nature *515*, 523–527.

Potter, C.J., Tasic, B., Russler, E.V., Liang, L., and Luo, L. (2010). The Q system: a repressible binary system for transgene expression, lineage tracing, and mosaic analysis. Cell *141*, 536–548.

Rajagopalan, S., Vivancos, V., Nicolas, E., and Dickson, B.J. (2000). Selecting a longitudinal pathway: Robo receptors specify the lateral position of axons in the Drosophila CNS. Cell *103*, 1033–1045.

Rolls, A., Shechter, R., London, A., Ziv, Y., Ronen, A., Levy, R., and Schwartz, M. (2007). Toll-like receptors modulate adult hippocampal neurogenesis. Nat. Cell Biol. *9*, 1081–1088.

Rose, D., Zhu, X., Kose, H., Hoang, B., Cho, J., and Chiba, A. (1997). Toll, a muscle cell surface molecule, locally inhibits synaptic initiation of the RP3 motoneuron growth cone in Drosophila. Development *124*, 1561–1571.

Silbering, A.F., Rytz, R., Grosjean, Y., Abuin, L., Ramdya, P., Jefferis, G.S., and Benton, R. (2011). Complementary function and integrated wiring of the evolutionarily distinct Drosophila olfactory subsystems. J. Neurosci. *31*, 13357–13375.

Simpson, J.H., Bland, K.S., Fetter, R.D., and Goodman, C.S. (2000). Short-range and long-range guidance by Slit and its Robo receptors: a combinatorial code of Robo receptors controls lateral position. Cell *103*, 1019–1032.

Spitzweck, B., Brankatschk, M., and Dickson, B.J. (2010). Distinct protein domains and expression patterns confer divergent axon guidance functions for Drosophila Robo receptors. Cell *140*, 409–420.

Stocker, R.F., Lienhard, M.C., Borst, A., and Fischbach, K.F. (1990). Neuronal architecture of the antennal lobe in Drosophila melanogaster. Cell Tissue Res. *262*, 9–34.

Sweeney, L.B., Couto, A., Chou, Y.H., Berdnik, D., Dickson, B.J., Luo, L., and Komiyama, T. (2007). Temporal target restriction of olfactory receptor neurons by Semaphorin-1a/PlexinA-mediated axon-axon interactions. Neuron *53*, 185–200.

Sweeney, L.B., Chou, Y.H., Wu, Z., Joo, W., Komiyama, T., Potter, C.J., Kolodkin, A.L., Garcia, K.C., and Luo, L. (2011). Secreted semaphorins from degenerating larval ORN axons direct adult projection neuron dendrite targeting. Neuron *72*, 734–747.

Takeda, K., Kaisho, T., and Akira, S. (2003). Toll-like receptors. Annu. Rev. Immunol. *21*, 335–376.

Xu, Y., Tao, X., Shen, B., Horng, T., Medzhitov, R., Manley, J.L., and Tong, L. (2000). Structural basis for signal transduction by the Toll/interleukin-1 receptor domains. Nature *408*, 111–115.

Zhu, H., and Luo, L. (2004). Diverse functions of N-cadherin in dendritic and axonal terminal arborization of olfactory projection neurons. Neuron *42*, 63–75.

Zipursky, S.L., and Sanes, J.R. (2010). Chemoaffinity revisited: dscams, protocadherins, and neural circuit assembly. Cell *143*, 343–353.

**Neuron, Volume *85***

## Supplemental Information

# Toll Receptors Instruct Axon and Dendrite Targeting and Participate in Synaptic Partner Matching in a *Drosophila* Olfactory Circuit

**Alex Ward, Weizhe Hong, Vincenzo Favaloro, and Liqun Luo**

# Inventory of Supplemental Information

**SUPPLEMENTAL FIGURES**

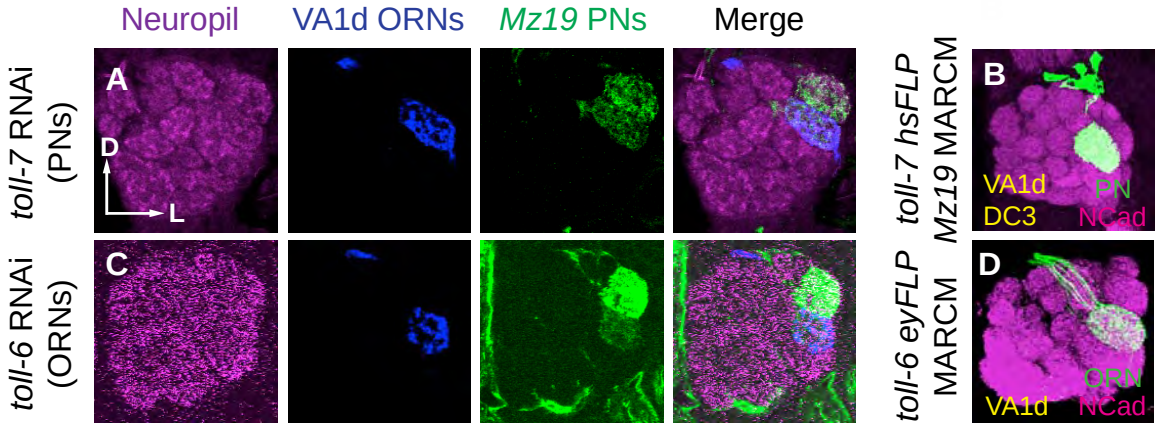


**Figure S1. Perturbation of Toll-7 in PNs or Toll-6 in ORNs Does Not Affect Wiring Specificity, Related to Figure 2 and Figure 4.**

(A) Dendrite targeting of *Mz19-GAL4*$^{+}$ PNs, and axon targeting of VA1d ORNs (labeled by *Or88a-myr-tdT* and pseudocolored in blue), are unaffected by *Mz19-GAL4*-based Toll-7 RNAi in PNs (mistargeting in N=0/50 antennal lobes tested).

(B) VA1d and DC3 PN dendrite targeting appears normal in *hsFLP Mz19-GAL4*-based *toll-7*$^{-/-}$ adNb MARCM clones (N=0/3 clones display mistargeting).

(C) Dendrite targeting of *Mz19-GAL4*$^{+}$ PNs, and axon targeting of VA1d ORNs, are unaffected by *Pebbled-GAL4*-based RNAi of Toll-6 in ORNs (mistargeting in 0/20 antennal lobes tested).

(D) VA1d ORN axon targeting is unperturbed in *eyFLP* MARCM clones in which *toll-6*$^{-/-}$ VA1d ORNs were labeled by *Or88a-GAL4* (mistargeting in 0/20 antennal lobes).

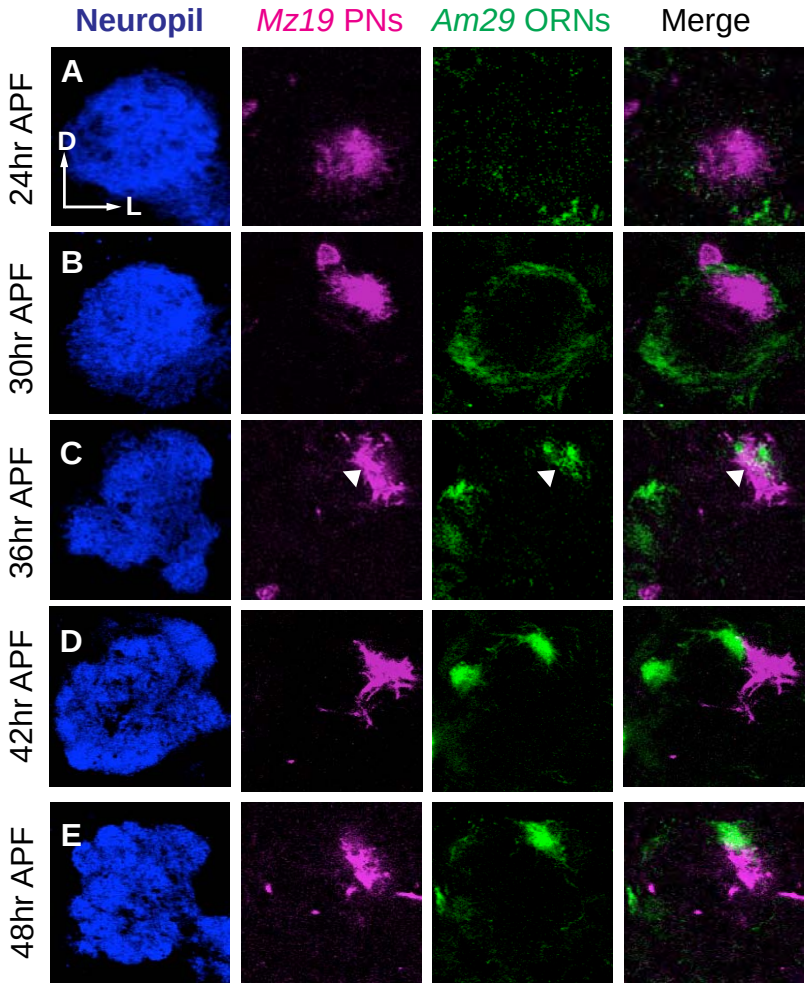


**Figure S2. PN Dendrites and ORN Axons Exhibit Dynamic Interactions at Early Pupal Stages, Related to Figure 2.**

Single confocal sections of pupal antennal lobes show neuropil staining in magenta, *Mz19-QF*$^{+}$ DA1 and VA1d PN dendrites (pseudocolored magenta), and *Am29-GAL4*$^{+}$ DM6 and DL4 ORN axons (green).

(A) At 24 hours APF, *Mz19-QF*$^{+}$ PNs elaborate dendrites in a ventral position occupying a relatively large antennal lobe territory. Incoming *Am29-GAL4*$^{+}$ ORN axons surround the antennal lobe and have begun invading the neuropil (not pictured in this confocal section).

(B) By 30 hours APF, DM6 and DL4 ORN axons begin to target specific positions in the antennal lobe. DA1 and VA1d PN dendrites have shifted dorsally, but are quite diffuse.

(C) DA1 and VA1d PN dendrites partially overlap with DL4 ORN axons at 36 hours APF in this confocal section (arrowheads).

(D) At 42 hours APF, DA1 and VA1d PN dendrites establish clear boundaries and no longer overlap with non-partner DL4 ORN axons.

(E) DA1 and VA1d PN dendrites and DL4 ORN axons have fully resolved into specific glomeruli by 48 hours APF and do not exhibit overlap (DM6 ORN axons not pictured in this confocal section).

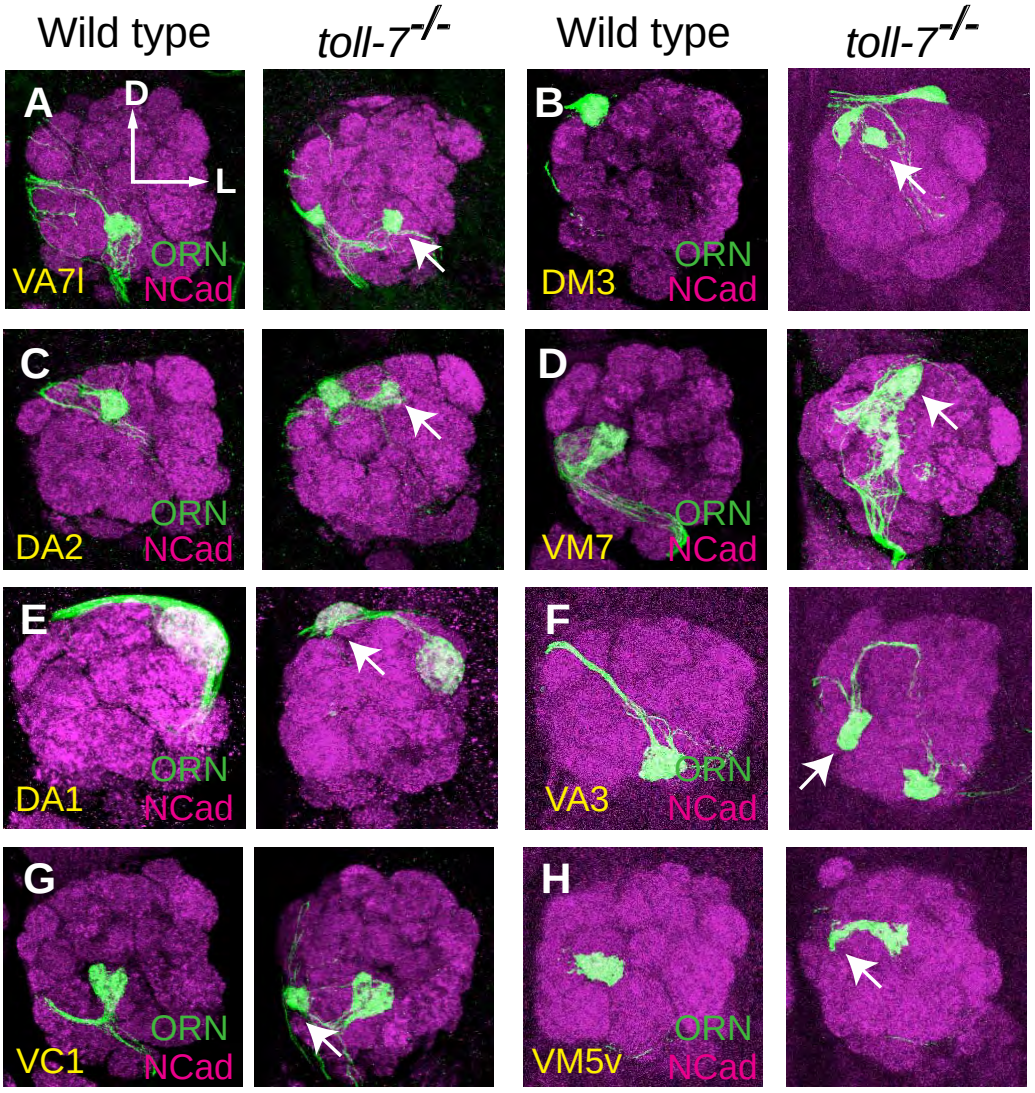


**Figure S3. Testing Toll-7 Function in Axon Targeting of Additional ORN Classes, Related to Figure 3.**

(A-H) All images are from confocal stack projections of *toll-7* whole animal mutant adult antennal lobes, with magenta showing neuropil staining and axons of specific ORN classes labeled by different *Or-GAL4* lines in green. Loss of *toll-7* causes severe axonal targeting defects in these eight ORN classes (arrows). Most classes mistarget axons to ectopic medial positions, but dorsal, ventral, and even lateral mistargeting was also observed in some cases. The penetrance of mistargeting in *toll-7* mutants are as follows (antennal lobe affected/antennal lobe examined): VA7l (24/32), DM3 (20/42), DA2 (11/16), VM7 (12/32), DA1 (12/20), VA3 (12/38), VC1 (12/30), and VM5v (3/6).

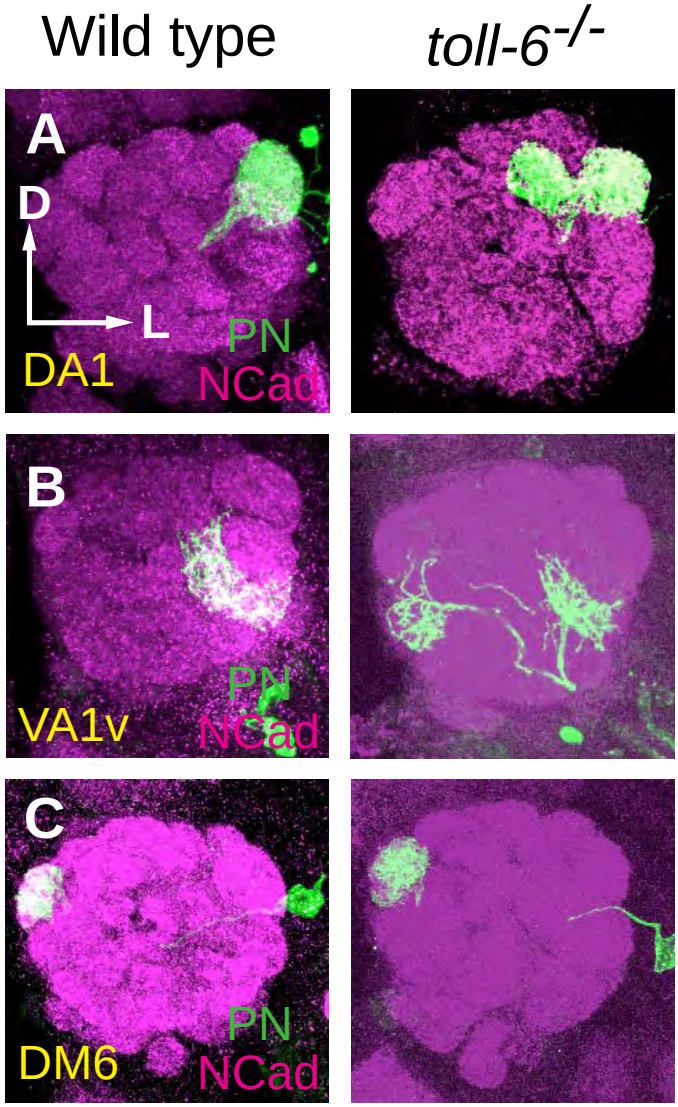


**Figure S4. Testing Toll-6 Function in Dendrite Targeting of Additional PN Classes, Related to Figure 5.**

All images are from confocal stack projections of adult antennal lobes showing *hsFLP* MARCM labeling of PN dendrites in green merged with neuropil staining in magenta.

(A) Left, *Mz19-GAL4*-labeled wild-type DA1 PNs in lateral neuroblast clones target dendrites to the DA1 glomerulus. Right, *toll-6*$^{-/-}$ DA1 clones exhibit low-penetrance local medial mistargeting (3/12 mistarget).

(B) Left, *7365-GAL4*-labeled wild-type VA1v PNs in ventral neuroblast clones target dendrites to the VA1v glomerulus. *toll-6*$^{-/-}$ VA1v clones mistarget dendrites to the medial antennal lobe (11/11 mistarget), similar to VA1d and DC3 PN MARCM clones (Figure 5B).

(C) Left, wild-type DM6 PN dendrites labeled by *853-GAL4* in single cell clones target the DM6 glomerulus. Right, *toll-6*$^{-/-}$ DM6 PN MARCM clones target dendrites normally (0/5 mistarget).

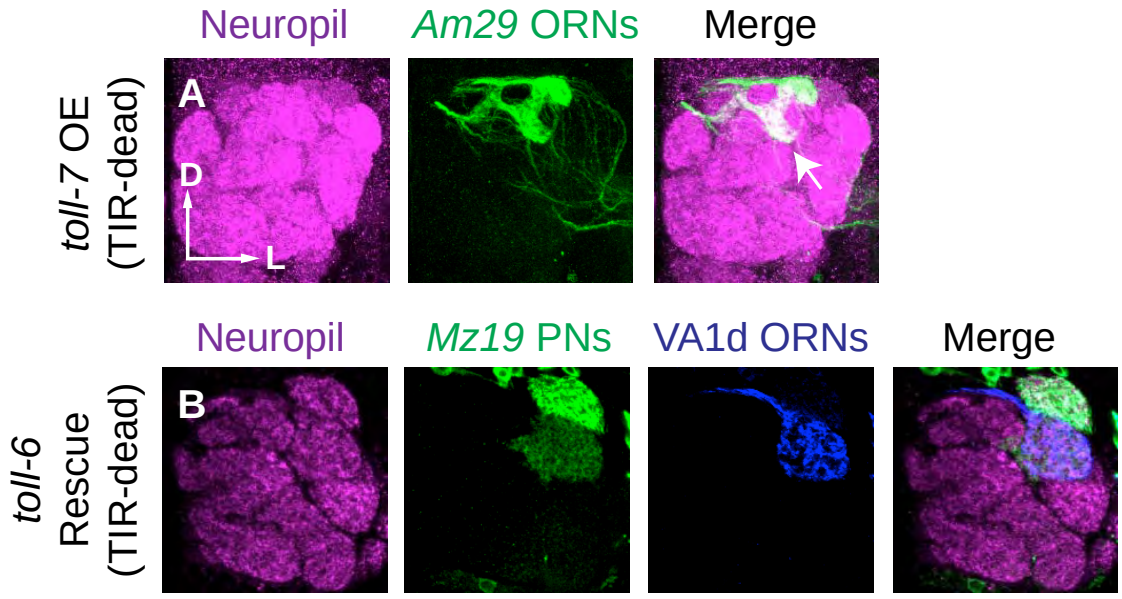


**Figure S5. TIR Domains of Toll-6 and Toll-7 Are Dispensable In Misexpression and Rescue Assays, Related to Figure 6.**

(A) Image shows neuropil staining in magenta and *Am29-GAL4*$^{+}$ DM6 and DL4 ORN axons in green. *Am29-GAL4*-based misexpression of a *UAS-toll-7* transgene in which conserved TIR domain amino acid residues were mutated (Toll-7 TIR-dead) exhibits lateral mistargeting of DM6 ORN axons (arrow; 8/8 mistarget).

(B) Image shows neuropil staining in magenta, *Or88a-myr*-tdT-labeled ORNs (pseudocolored blue) and *Mz19-GAL4*$^{+}$ PNs in green. *Mz19-GAL4*-based misexpression of a *UAS-toll-6* TIR-dead transgene rescues *toll-6* mutant PN dendrite and ORN axon mistargeting phenotypes. (Of the 20 antennal lobes examined, ORN axons mistarget in 1/20, PN dendrites mistarget in 0/20).

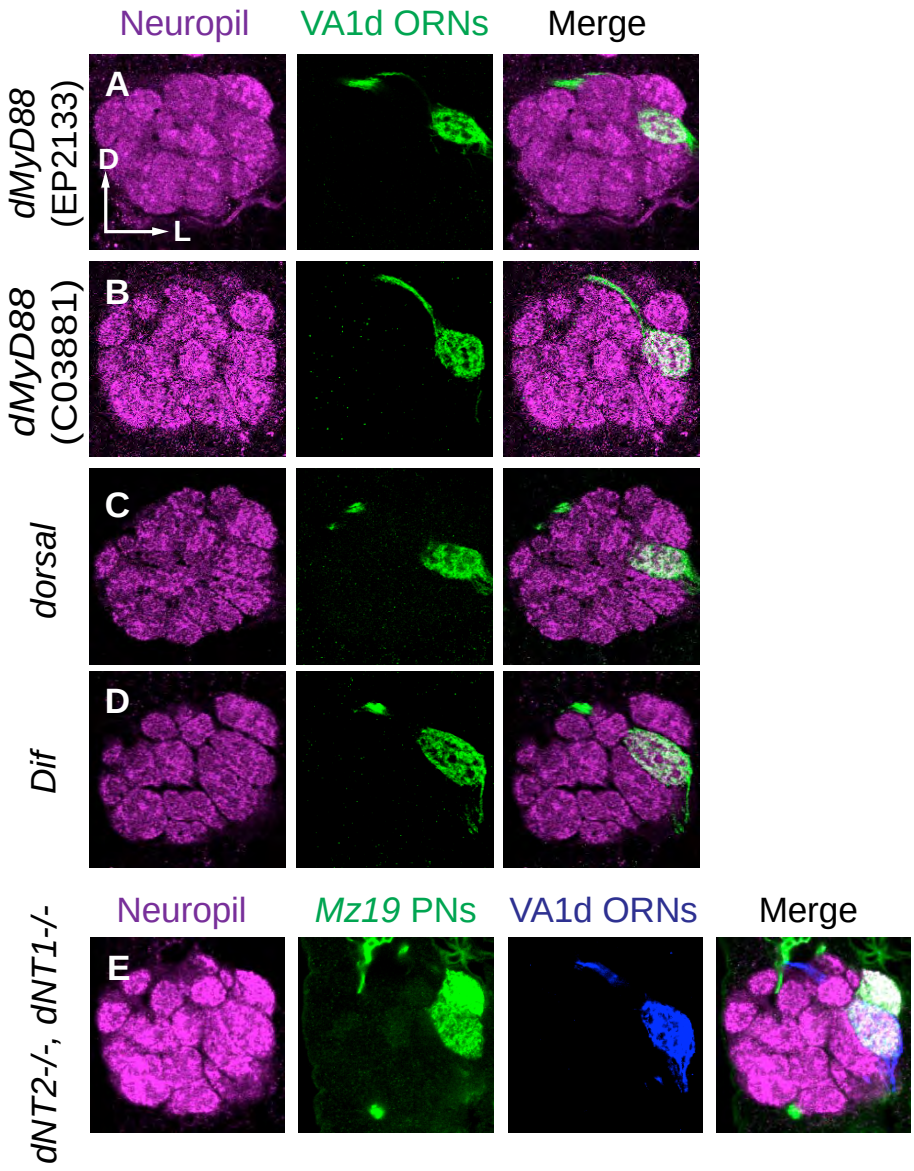


**Figure S6. Canonical Toll Pathway Components Are Not Required for VA1d ORN Axon and PN Dendrite Targeting, Related to Figure 6.**

Panels A-D show a single confocal section of adult antennal lobes, with neuropil staining in magenta and VA1d ORNs labeled by Or88a-mCD8GFP (green). In panel E, *Mz19-GAL4*$^{+}$ DA1, VA1d, and DC3 PNs are labeled in green and VA1d ORNs are labeled by *Or88a-myr-tdT* (pseudocolored blue).

(A-D) VA1d ORN axon targeting appears normal in the canonical Toll-signaling mutants *dMyD88* (two alleles, *EP2133* and *C03881*), *dorsal*$^{1}$, and *Dif*$^{1}$ (0/8, 0/8, 0/6, 0/4 mistarget for panels A-D, respectively).

(E) DA1 and VA1d PN dendrites, and VA1d ORN axons, target normally in *dNT2*, *dNT1* double mutant flies (0/18 mistarget). DC3 PN dendrites are not pictured in this section.

## SUPPLEMENTAL EXPERIMENTAL PROCEDURES

### Mutants and Transgenes

$Mz19^{+}$ PN dendrites were labeled by *Mz19-QF* and *Mz19-GAL4* (Hong et al., 2012). *Mz19-GAL4* labels VA1d, DC3, and DA1 PNs; *Mz19-QF* labels DA1 PNs in all samples, VA1d PNs in a subset of samples, and does not label DC3 PNs. VM6 PNs were labeled using the Janelia Farm GAL4 collection line *71D09-GAL4* (Jenett et al., 2012). Ventral-lineage VA1v PN dendrites were labeled by the Kyoto DGRC line *NP7365-GAL4* (Tanaka et al., 2012). DM6 PN dendrites were labeled by the InSITE line *853-GAL4* (Gohl et al., 2011). *Or-GAL4* and *Or-mCD8GFP* lines have been previously described (Couto et al., 2005; Fishilevich and Vosshall, 2005; Komiyama et al., 2004). DM6 and DL4 ORN axons were labeled by *Am29-GAL4* (Endo et al., 2007; Joo et al., 2013). Tissue-specific *toll-6* expression was assessed using the *toll-6* enhancer trap *D42-GAL4* (McIlroy et al., 2013) in conjunction with *UAS>stop>mCD8GFP* (Hong et al., 2009), *eyFLP* (Hummel et al., 2003) and *GH146-FLP* (Potter et al., 2010). *Pebbled-GAL4* (Sweeney et al., 2007) and *GH146-GAL4* (Stocker et al., 1997) were used for tissue-specific RNAi of *toll-6* and *toll-7*. *Or88a-myr-tdTomato* (H. Zhu and L. L., unpublished data) and *Or88a-ratCD2* (Berdnik et al., 2006) were used for labeling of VA1d ORNs. *QUAS-mCD8GFP* (Potter et al., 2010) was used as a reporter in the RNAi screen. *UAS-mCD8GFP* has been previously described (Lee and Luo, 1999) as has *10XUAS-IVS-mtdT* (Pfeiffer et al., 2010). *UAS-dcr2* was used to enhance RNAi efficiency in all RNAi experiments (Dietzl et al., 2007).

Loss of function experiments used the following mutant alleles and RNAi lines: for *toll-7* RNAi we used the VDRC lines 6541 and 24473 (Dietzl et al., 2007) and the TRiP collection line HM05230 (Ni et al., 2009); for *toll-6* RNAi we used VDRC lines 928, 27102, and 108907 (Dietzl et al., 2007); the $toll\text{-}6^{Ex13}$ null allele has been previously described (Yagi et al., 2010); we made a $toll\text{-}7^{AW1}$ null allele by *FLP*-mediated *trans* excision (Parks et al., 2004) of two flanking PiggyBac FRT-containing insertions PBac{WH}F04328 and PBac{RB}e00402 (this allele also removes a recently annotated gene *CG44569*); the canonical Toll-pathway mutants tested include $dMyD88^{EP2133}$ (generously provided by S. Cherry, Tauszig-Delamasure et al., 2002), $dMyD88^{C03881}$ (generously provided by J.M. Reichhart, Kambris et al., 2003), $dorsal^{1}$ (Nüsslein-Volhard, 1979), $Dif^{1}$ (Rutschmann et al., 2000), two *spz* alleles $spz^{2}$ and $spz^{3}$ (Anderson, 1984). $dNT1^{41}$ (Zhu et al., 2008) was kindly provided by A. Hidalgo. We made the $dNT2^{AW18}$ null allele by using *FLP*-mediated *trans* excision (Parks et al., 2004) of two flanking PiggyBac FRT-containing insertions PBac{WH}F04949 and PBac{XP}d05170 (this allele also removes the gene *CG43444*).

Rescue and overexpression experiments: *UAS* transgenes for all nine *Drosophila* Toll-family receptors (kindly provided by Y. Yagi) have been previously described (Yagi et al., 2010); *UAS-toll-6Δcyto* and *UAS-toll-7Δcyto* were generated as follows: the extracellular domain and transmembrane domain coding regions for each *toll-6* and *toll-7* were subcloned into Invitrogen pENTR/D-TOPO donor vectors. The donor vector was recombined by L/R reaction with a destination vector containing the GFP coding sequence in frame at the 3' end of the attB site. The L/R reaction produced a construct that encodes the extracellular and transmembrane domains of Toll-6 (or Toll-7) fused with GFP at the C-terminus (pToll-6Δcyto-GFP and pToll-7Δcyto-GFP). *UAS-toll-6Δcyto* and *UAS-toll-7Δcyto* transgenic flies were made by P-element-mediated random insertion. *UAS-toll-6(TIR-dead)* and *UAS-toll-7(TIR-dead)* flies were made by mutagenesis of two conserved TIR domain residues that are critical for TIR function: an arginine in the BB loop and a glutamate in the αA helix (Xu et al., 2000). Briefly, the full-length coding

sequence of *toll-6* and *toll-7* were subcloned into Invitrogen pENTR/D-TOPO donor vectors. The donor vector was recombined by L/R reaction with a destination vector containing a FLAG tag, a 3XHA epitope, and a 10XHIS tag, in frame (in that order), at the 3' end of the attB site. The L/R reaction produced a construct that encodes a Toll-6 (or Toll-7) C-terminal FLAG-3XHA-10XHIS fusion protein upon expression (i.e., *pToll-6-FLAG-3XHA-10XHIS* and *pToll-7-FLAG-3XHA-10XHIS*). The conserved glutamate and arginine residues in Toll-6 and Toll-7 were determined by Blast comparison of the *Drosophila* Toll-1 TIR domain, in which these residues have been previously studied (Xu et al., 2000), with the TIR domains of Toll-6 and Toll-7. Based on this analysis, we used the Stratagene QuikChange Site-Directed Mutagenesis kit to mutate Toll-6 residues E1136R and R1148E and the Toll-7 residues E1121R and R1134E in the pToll-6-FLAG-3XHA-10XHIS and pToll-7-FLAG-3XHA-10XHIS constructs to make pToll-6TIRdead and pToll-7TIRdead, respectively. *pToll-6TIRdead* and *pToll-7TIRdead* were injected into the P40 landing site by integrase-mediated transgenesis. All constructs were verified by sequencing.

## SUPPLEMENTAL REFERENCES

Anderson, K.V., Nüsslein-Volhard, C. (1984). Genetic analysis of dorsal-ventral embryonic pattern in Drosophila. (New York: Macmillan).

Berdnik, D., Chihara, T., Couto, A., and Luo, L. (2006). Wiring stability of the adult Drosophila olfactory circuit after lesion. J Neurosci *26*, 3367-3376.

Couto, A., Alenius, M., and Dickson, B.J. (2005). Molecular, anatomical, and functional organization of the Drosophila olfactory system. Curr Biol *15*, 1535-1547.

Dietzl, G., Chen, D., Schnorrer, F., Su, K.C., Barinova, Y., Fellner, M., Gasser, B., Kinsey, K., Oppel, S., Scheiblauer, S., *et al.* (2007). A genome-wide transgenic RNAi library for conditional gene inactivation in Drosophila. Nature *448*, 151-156.

Endo, K., Aoki, T., Yoda, Y., Kimura, K., and Hama, C. (2007). Notch signal organizes the Drosophila olfactory circuitry by diversifying the sensory neuronal lineages. Nat Neurosci *10*, 153-160.

Fishilevich, E., and Vosshall, L.B. (2005). Genetic and functional subdivision of the Drosophila antennal lobe. Curr Biol *15*, 1548-1553.

Gohl, D.M., Silies, M.A., Gao, X.J., Bhalerao, S., Luongo, F.J., Lin, C.C., Potter, C.J., and Clandinin, T.R. (2011). A versatile in vivo system for directed dissection of gene expression patterns. Nature methods *8*, 231-237.

Hong, W., Mosca, T.J., and Luo, L. (2012). Teneurins instruct synaptic partner matching in an olfactory map. Nature *484*, 201-207.

Hong, W., Zhu, H., Potter, C.J., Barsh, G., Kurusu, M., Zinn, K., and Luo, L. (2009). Leucine-rich repeat transmembrane proteins instruct discrete dendrite targeting in an olfactory map. Nat Neurosci *12*, 1542-1550.

Hummel, T., Vasconcelos, M.L., Clemens, J.C., Fishilevich, Y., Vosshall, L.B., and Zipursky, S.L. (2003). Axonal targeting of olfactory receptor neurons in Drosophila is controlled by Dscam. Neuron *37*, 221-231.

Jenett, A., Rubin, G.M., Ngo, T.T., Shepherd, D., Murphy, C., Dionne, H., Pfeiffer, B.D., Cavallaro, A., Hall, D., Jeter, J., *et al.* (2012). A GAL4-driver line resource for Drosophila neurobiology. Cell reports *2*, 991-1001.

Joo, W.J., Sweeney, L.B., Liang, L., and Luo, L. (2013). Linking cell fate, trajectory choice, and target selection: genetic analysis of Sema-2b in olfactory axon targeting. Neuron *78*, 673-686.

Kambris, Z., Bilak, H., D'Alessandro, R., Belvin, M., Imler, J.L., and Capovilla, M. (2003). DmMyD88 controls dorsoventral patterning of the Drosophila embryo. EMBO reports *4*, 64-69.

Komiyama, T., Carlson, J.R., and Luo, L. (2004). Olfactory receptor neuron axon targeting: intrinsic transcriptional control and hierarchical interactions. Nat Neurosci *7*, 819-825.

Lee, T., and Luo, L. (1999). Mosaic analysis with a repressible cell marker for studies of gene function in neuronal morphogenesis. Neuron *22*, 451-461.

McIlroy, G., Foldi, I., Aurikko, J., Wentzell, J.S., Lim, M.A., Fenton, J.C., Gay, N.J., and Hidalgo, A. (2013). Toll-6 and Toll-7 function as neurotrophin receptors in the Drosophila melanogaster CNS. Nat Neurosci *16*, 1248-1256.

Ni, J.Q., Liu, L.P., Binari, R., Hardy, R., Shim, H.S., Cavallaro, A., Booker, M., Pfeiffer, B.D., Markstein, M., Wang, H., *et al.* (2009). A Drosophila resource of transgenic RNAi lines for neurogenetics. Genetics *182*, 1089-1100.

Nüsslein-Volhard, C. (1979). Maternal effect mutations that affect the spatial coordinates of the embryo of Drosophila melanogaster. Subtelny, Konigsberg, 185-211.

Parks, A.L., Cook, K.R., Belvin, M., Dompe, N.A., Fawcett, R., Huppert, K., Tan, L.R., Winter, C.G., Bogart, K.P., Deal, J.E., *et al.* (2004). Systematic generation of high-resolution deletion coverage of the Drosophila melanogaster genome. Nat Genet *36*, 288-292.

Pfeiffer, B.D., Ngo, T.T., Hibbard, K.L., Murphy, C., Jenett, A., Truman, J.W., and Rubin, G.M. (2010). Refinement of tools for targeted gene expression in Drosophila. Genetics *186*, 735-755.

Potter, C.J., Tasic, B., Russler, E.V., Liang, L., and Luo, L. (2010). The Q system: a repressible binary system for transgene expression, lineage tracing, and mosaic analysis. Cell *141*, 536-548.

Rutschmann, S., Jung, A.C., Hetru, C., Reichhart, J.M., Hoffmann, J.A., and Ferrandon, D. (2000). The Rel protein DIF mediates the antifungal but not the antibacterial host defense in Drosophila. Immunity *12*, 569-580.

Stocker, R.F., Heimbeck, G., Gendre, N., and de Belle, J.S. (1997). Neuroblast ablation in Drosophila P[GAL4] lines reveals origins of olfactory interneurons. Journal of neurobiology *32*, 443-456.

Sweeney, L.B., Couto, A., Chou, Y.H., Berdnik, D., Dickson, B.J., Luo, L., and Komiyama, T. (2007). Temporal target restriction of olfactory receptor neurons by Semaphorin-1a/PlexinA-mediated axon-axon interactions. Neuron *53*, 185-200.

Tanaka, N.K., Endo, K., and Ito, K. (2012). Organization of antennal lobe-associated neurons in adult Drosophila melanogaster brain. J Comp Neurol *520*, 4067-4130.

Tauszig-Delamasure, S., Bilak, H., Capovilla, M., Hoffmann, J.A., and Imler, J.L. (2002). Drosophila MyD88 is required for the response to fungal and Gram-positive bacterial infections. Nature immunology *3*, 91-97.

Xu, Y., Tao, X., Shen, B., Horng, T., Medzhitov, R., Manley, J.L., and Tong, L. (2000). Structural basis for signal transduction by the Toll/interleukin-1 receptor domains. Nature *408*, 111-115.

Yagi, Y., Nishida, Y., and Ip, Y.T. (2010). Functional analysis of Toll-related genes in Drosophila. Development, growth & differentiation *52*, 771-783.

Zhu, B., Pennack, J.A., McQuilton, P., Forero, M.G., Mizuguchi, K., Sutcliffe, B., Gu, C.J., Fenton, J.C., and Hidalgo, A. (2008). Drosophila neurotrophins reveal a common mechanism for nervous system formation. PLoS Biol *6*, e284.